The Company of Biologists

RESEARCH ARTICLE

A SUMOylation-dependent switch of RAB7 governs intracellular life and pathogenesis of *Salmonella* Typhimurium

Gayatree Mohapatra[1,2], Preksha Gaur[1], Prabhakar Mujagond[1,*], Mukesh Singh[3,*], Sarika Rana[1,2], Shivendra Pratap[1], Navneet Kaur[4], Smriti Verma[5], Vengadesan Krishnan[1], Nirpendra Singh[1] and C. V. Srikanth[1,‡]

ABSTRACT

Salmonella Typhimurium is an intracellular pathogen that causes gastroenteritis in humans. Aided by a battery of effector proteins, *S.* Typhimurium resides intracellularly in a specialized vesicle, called the *Salmonella*-containing vacuole (SCV) that utilizes the host endocytic vesicular transport pathway (VTP). Here, we probed the possible role of SUMOylation, a post-translation modification pathway, in SCV biology. Proteome analysis by complex mass-spectrometry (MS/MS) revealed a dramatically altered SUMO-proteome (SUMOylome) in *S.* Typhimurium-infected cells. RAB7, a component of VTP, was key among several crucial proteins identified in our study. Detailed MS/MS assays, *in vitro* SUMOylation assays and structural docking analysis revealed SUMOylation of RAB7 (RAB7A) specifically at lysine 175. A SUMOylation-deficient RAB7 mutant (RAB7^{K175R}) displayed longer half-life, was beneficial to SCV dynamics and functionally deficient. Collectively, the data revealed that RAB7 SUMOylation blockade by *S.* Typhimurium ensures availability of long-lived but functionally compromised RAB7, which was beneficial to the pathogen. Overall, this SUMOylation-dependent switch of RAB7 controlled by *S.* Typhimurium is an unexpected mode of VTP pathway regulation, and unveils a mechanism of broad interest well beyond *Salmonella*–host crosstalk.

This article has an associated First Person interview with the first author of the paper.

KEY WORDS: *Salmonella*, *Salmonella*-containing vacuole, Vesicular transport system, RAB7, PTMs, SUMOylation

INTRODUCTION

Salmonella enterica serovar Typhimurium is a facultative Gram-negative pathogen causing food-borne gastroenteritis in humans (Bhan et al., 2005). Symptoms include abdominal cramps, diarrhoea, fever and vomiting. In healthy individuals, the disease is self-limiting and the individual recovers in 5–7 days. In the case of infants and immune-compromised individuals, however, the disease outcome may involve diverse clinical presentations and even be life-threatening. The bacterium enters the human body through contaminated food or water, and is able to overcome gastric acidic pH to reach intestinal epithelial cells, the prime targets of invasion. Using a range of secreted effector proteins encoded by *Salmonella* pathogenicity island I and II (*SPI-I* and *SPI-II*), which includes a multi-protein secretory apparatus (Galán, 1996), *S.* Typhimurium enters intestinal epithelial cells (Galán, 1996; Srikanth et al., 2011). The concerted action of these effectors such as SopE, SopE2, SipA and SipC drives massive actin rearrangement, membrane ruffling and formation of lamellapodial extensions in the host cells that engulf the bacterium into a membrane-enclosed intracellular compartment called the *Salmonella*-containing vacuole (SCV) (Bakowski et al., 2008). Sequestration of bacterium within the SCV is critical since it enables evasion of host defence and allows rapid multiplication. Key aspects of SCV survival and maintenance are governed by the concerted action of *SPI-I*- and *SPI-II*-encoded effectors (Forest et al., 2010). The effectors highjack the vesicular endocytic transport pathway (VTP) components, interfere with their recruitment at the SCV membrane and thereby ensure stability of the SCV (Brumell and Grinstein, 2004). Newly formed SCVs resemble early endosomes, with their membranes decorated by early endosomal markers such as EEA1, SNX1 and RAB5. At later time points, SCVs acquire late markers RAB7 and lysosomal glycoproteins LAMP1, LAMP2 and vATPases (Steele-Mortimer et al., 1999; Madan et al., 2012; Baldeón et al., 2001; Harrison et al., 2004). Thus, SCVs interact closely with the host VTP, and this interaction results in luminal acidification and enrichment of lysosomal glycoproteins (Drecktrah et al., 2007). However, unlike a regular late endosome, the SCVs do not accumulate lysosomal hydrolases and therefore have a less potent bactericidal environment (McGourty et al., 2012). This is mainly due to a selective acquisition of the correct set of VTP proteins at the SCV, and probably with their altered functions. Collectively, these events are determined by the action of *S.* Typhimurium effector proteins.

RAB7, a Ras family small GTPase, participates in multiple processes involving vesicular trafficking including autophagy and acts as a master regulator of these processes. RAB7 is utilized by *S.* Typhimurium for SCV maturation, stabilization and subcellular positioning (Brumell and Grinstein, 2004; Harrison et al., 2004; D'Costa et al., 2015). An incoming cargo destined for lysosomal fusion remains in the endosome, and slowly undergoes a maturation process involving shedding of RAB5 and simultaneous acquisition of RAB7 (Rink et al., 2005). However, pathogens like *S.* Typhimurium manipulate endocytic trafficking and modify the fate of the phagosome (D'Costa et al., 2015; Madan et al., 2008). In addition to these events, SCV maturation requires the formation of long tubular filaments that emanate from the SCV called

[1]Laboratory of Gut Inflammation and Infection Biology, Regional Centre for Biotechnology NCR Biotech Science Cluster 3rd Milestone, Faridabad-Gurgaon Expressway, Faridabad – 121 001 Haryana (NCR Delhi), India. [2]Manipal Acadamy of Higher Education, Manipal, Karnataka 576104, India. [3]Pediatric Biology Centre, Translational Health Science and Technology Institute, NCR Biotech Science Cluster, 3rd Milestone, Faridabad – Gurgaon Expressway, PO box #04, Faridabad – 121001 Haryana, India. [4]Department of Biochemistry and Molecular Biology, University of Nebraska Medical Centre, Omaha, NE 68198, USA. [5]Mucosal Immunology and Biology Research Center, Massachusetts General Hospital, Building 114, 16th Street, Charlestown, MA 02129, USA.
*These authors contributed equally to this work

‡Author for correspondence (cvsrikanth@rcb.res.in)

V.K., 0000-0002-8083-0121; C.V.S., 0000-0001-9381-1213

Salmonella-induced filaments (SIFs). The SIFs are also known to be decorated by LAMP1, and their formation is necessary for the stability of SCV, with the event coordinated by effector proteins including SifA, SseJ and others, in association with RAB7 (Ohlson et al., 2008). During infection, SifA mutant *S.* Typhimurium are unable to sequester themselves in an SCV and usually escape into the host cytoplasm to undergo uncontrolled division (Beuzón et al., 2000). Previous reports have demonstrated that *S.* Typhimurium uses SifA to regulate RAB7, which in turn is a crucial regulator of VTP. *S.* Typhimurium orchestrates SCV stability by recruiting the RAB7 effector protein PLEKHM1, which is otherwise involved in dynein-mediated retrograde transport of the late endosome to autophagosomes, to SCV membrane (McEwan et al., 2015). PLEKHM1 is a multifunctional adapter protein that directly binds and regulates RAB7. Being a master regulator of endolysosomal trafficking, RAB7 activation and its context is crucial for the fate of the vesicle it belongs to, whether it is part of the late endosome or of the SCV. The precise location of RAB7 and its interacting partners determines these fates. A series of post-translational modifications (PTMs) are known to affect RAB7 and add to the layers of regulation of its function. These PTMs include palmitoylation, phosphorylation and ubiquitylation (Modica et al., 2017; Shinde and Maddika, 2016; Song et al., 2016). However, the specificities and details of these PTM events are not fully understood in the context of *S.* Typhimurium infection.

A recent report from our lab established that SUMOylation, a PTM pathway, plays a key role in *S.* Typhimurium pathogenesis (Verma et al., 2015). In humans, the SUMO pathway involves three SUMO protein isoforms, SUMO1, SUMO2 and SUMO3. SUMO2 and SUMO3 differ by three amino acids, whereas both share 47% sequence similarity with SUMO1. SUMO-modification of a target protein occurs at the lysine residue within a SUMO motif denoted by ΨKXD/E, where Ψ is a hydrophobic amino acid, K is the target lysine that gets modified, X is any amino acid and D/E are aspartic acid or glutamic acid. The modification can happen either as a single SUMO addition (usually SUMO1) (Sampson et al., 2001) or a chain of additions (usually SUMO2 and/or SUMO3) (Vertegaal et al., 2006). The process of SUMOylation involves machinery consisting of an E1 activating enzyme (SAE1 or SAE2), an E2 conjugating enzyme (UBC9, also known as UBE2I) and one of several E3 ligases (PIAS1, PIAS2, PIAS4 and PIASy). Once SUMO-modified, the protein can interact with novel partners, specifically those harbouring one or more SUMO-interacting motifs (SIMs). DeSUMOylation involves several cysteine proteases also called deSUMOylases or sentrin-specific proteases (SENPs). SUMOylation processes act as molecular switches allowing proteins to carry out a variety of functions (Flotho and Melchior, 2013; Mustfa et al., 2017). In an earlier work, we reported SUMOylation to be important for *S.* Typhimurium infection (Verma et al., 2015), although its exact role in the intracellular life of the bacteria remains unexplored. In the present work, we carried out experiments to further understand the precise role of SUMOylation in the intracellular life of *Salmonella*. We demonstrate a novel 'SUMOylation-switch' that regulates RAB7 function, and reveal its significance in the intracellular life of *S.* Typhimurium.

RESULTS
Salmonella reprograms the host SUMOylome during infection
We have reported previously that infection of intestinal epithelial cells with *S.* Typhimurium led to a downregulation of host SUMOylation machinery, and that the SUMOylation alteration facilitated intracellular multiplication of bacteria (Verma et al.,

2015). To further understand the effect of SUMOylation on the intracellular life of *S.* Typhimurium, in the current study, we checked the effect of experimental perturbation of host cellular SUMOylation status at later stages of infection. Transient transfection of HCT-8 intestinal epithelial cells with overexpression of the components of SUMOylation machinery such as SUMO1 (using plasmid pEYFP SUMO1), SUMO2 [using plasmid pcDNA3 HA-SUMO2, representative of SUMO2 and SUMO3 (SUMO2/3 hereafter)] or UBC9 (using plasmid pcDNA3/UBC9), led to an overall increase in SUMOylation compared to cells that were transfected with vector control (Fig. S1A,B). Expression of these components resulting in an activation of SUMOylation machinery, as had been demonstrated by others and our group in earlier studies (Ayaydin and Dasso, 2004; Verma et al., 2015). These cells with activated SUMOylation machinery were then infected with *S.* Typhimurium (lab strain SL1344) and intracellular bacterial load was estimated by gentamicin protection assay. Compared to cells transfected with vector alone (pEYFP-C1), those transfected with components of SUMOylation pathway (UBC9, SUMO1 or SUMO2/3) led to significant inhibition of *S.* Typhimurium colony forming units (CFUs) at 7 h and 24 h post-infection (hpi) (Fig. 1A,B). However, at 2 hpi there was no difference in number of CFUs between the SUMO-activated and control cells, indicating that entry of bacteria to the epithelial cell was unaffected by SUMOylation alteration (Fig. S1C). Compared to control cells (pEYFP-C1VC), in SUMO upregulated cells, *S.* Typhimurium multiplication was significantly compromised by decreases of ∼26%, ∼39% and ∼58% in case of UBC9, SUMO1 and SUMO2/3, respectively. Among the two SUMO isoform groups, the effect of SUMO2/3 was observed to be more pronounced. Thus, these data led us to conclude that experimental SUMOylation upregulation is inhibitory to the intracellular multiplication of *S.* Typhimurium. The intracellular life of *S.* Typhimurium depends on stability of the SCV, which in turn depends on formation of SIFs. To examine the role of the SUMOylation pathway in the formation of SIFs we checked the status of SIFs in SUMO2/3- and UBC9-activated HeLa cells. In control cells that were infected with *S.* Typhimurium for 7 h, we were able to observe SIFs by staining for lysosomal glycoprotein, LAMP1 (Fig. 1C, yellow arrows). However, upon SUMO upregulation, the proportion of cells containing SIFs (as seen by LAMP1 staining) was drastically reduced compared to infected cells transfected with vector control (Fig. 1C,D; Fig. S1C,D). Taken together, these data led us to conclude that SUMOylation plays a critical role in intracellular life of *S.* Typhimurium and SIF formation.

Salmonella-infected cells have an altered SUMOylome
In order to understand the connection between SUMOylation and *Salmonella* in greater detail, we next set out to decipher the infection-specific SUMO-conjugated proteome (SUMOylome) by comparative mass spectrometry. Our methodology, a modified version of that developed by Bruderer et al. (2011), relied on the capacity of a RING finger protein, RNF4, to bind to SUMO2/3-conjugated proteins. The presence of multiple SIMs in RNF4 enables a strong interaction with SUMOylated proteins. Thus, a construct encoding wild-type RNF4 was cloned as a GST-tagged version (named RNF4 WT in *E. coli* Rosetta strain, WT-RNF4). The tagged protein was expressed and purified as a GST-conjugated protein. Separately, a mutant version of GST-tagged RNF4 (hereafter SMUT-RNF4) devoid of SIMs was also purified. Full-length plasmids encoding WT-RNF4 and SMUT-RNF4 were sequenced to ensure that the constructs were correct. Expression of SMUT-RNF4, which is devoid of SUMO-target interaction, was
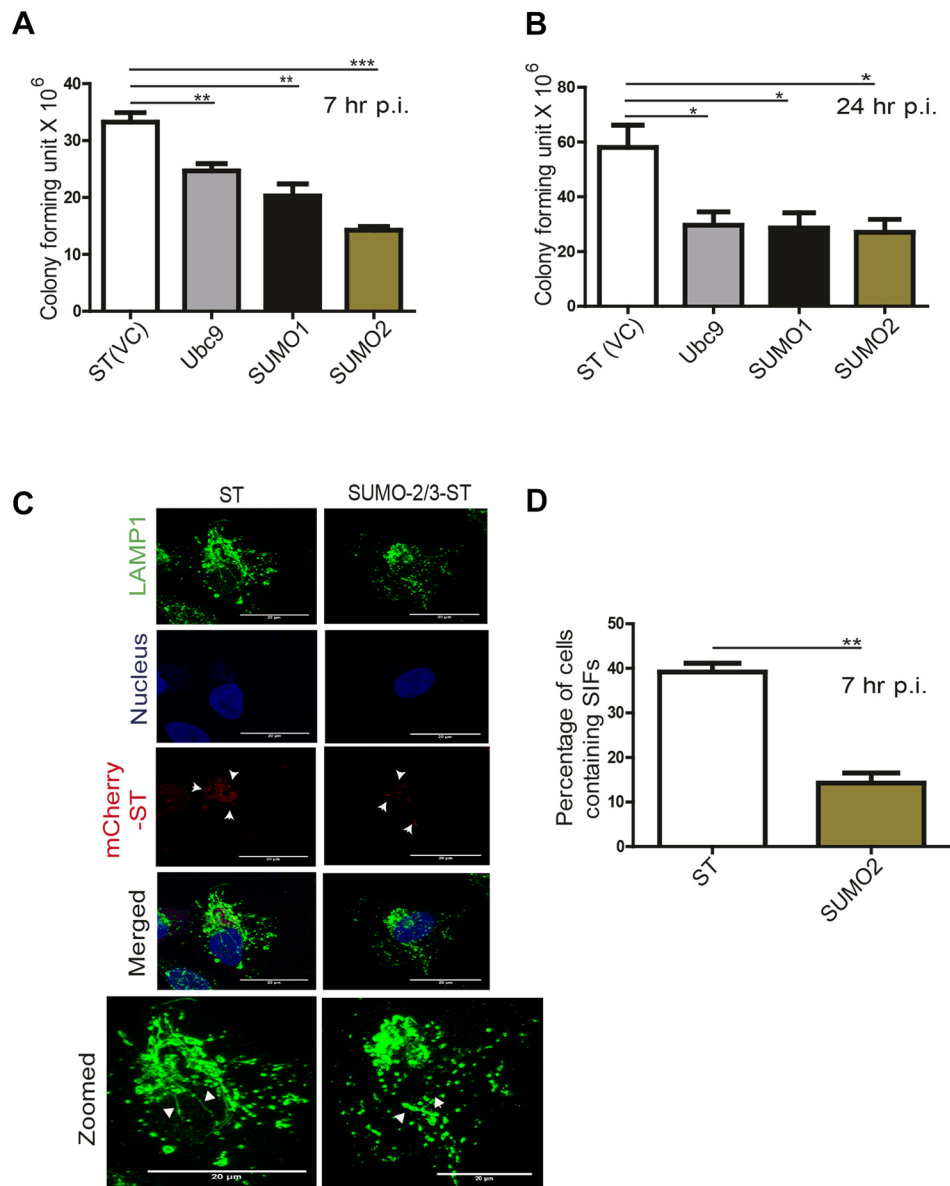
Fig. 1. Host SUMOylation status affects S. Typhimurium infection. (A,B) Gentamicin protection assay was performed in HCT-8 cells transfected with vector control (VC) plasmids or those encoding SUMO1, SUMO2/3 or UBC9, and infected with S. Typhimurium (ST) for 7 h (A) or 24 h (B). Colony forming units (CFUs) obtained were plotted for the indicated samples. Mean±s.e.m. from three independent experiments was included in the plots. (C) Confocal microscopic images of HeLa cells transfected with pcDNA HA-SUMO2 plasmid, followed by infection with S. Typhimurium expressing mCherry for 7 h and immunostained for LAMP1 to visualize Salmonella-induced filaments (SIFs). SIFs (yellow arrows) were visualized in 30 individual cells (N=30) in each case. Scale bars: 20 µm. Zoomed image of the area of interest is also represented (bottom panel). S. Typhimurium are marked with white arrows. (D) Quantitative representation of mean ±s.e.m SIFs (percentage) from three independent experiments is plotted. *$P \leq 0.05$, **$P \leq 0.01$, ***$P \leq 0.001$ by unpaired Student's t-test. Data is a representative of at least three independent biological experiments.

used to eliminate non-specific binders. The purified WT-RNF4 and SMUT-RNF4 bound to glutathione beads formed an affinity system through which we passed the lysates of S. Typhimurium-infected or control epithelial cells (Fig. 2A). The protein mixture bound to WT-RNF4 and SMUT-RNF4 was eluted by using buffer containing a high concentration of SIM peptide. Equal volumes of the eluted samples were run on SDS-PAGE, and Coomassie staining revealed detectable differences in samples from control versus S. Typhimurium lanes (Fig. 2A, bottom panel). These differences were also seen by a SUMO2/3 immunoblotting (Fig. 2B). Notably the bands from SMUT-RNF4 purified fraction were comparatively fainter, indicating decreased efficiency of binding with bona-fide partners in the absence of SIM domains (Fig. 2A,B).

The purified samples were concentrated, de-salted, processed and subjected to electrospray ionisation (ESI) mass spectrometry. The obtained list of proteins that were unique to the WT-RNF4 sample, but not bound to SMUT-RNF4, were identified as the true SUMO-conjugated proteome. Post-analysis, we identified 60 different proteins in uninfected samples and 147 proteins in S.

Typhimurium-infected samples (Fig. 2D). The details of the identified proteins are shown in Venn diagrams (Fig. 2C,D). For further validation, we ran these samples through CUCKOO SUMO motif and SIM identification software (http://sumosp.biocuckoo.org/online.php) and picked only those candidates that harboured either a SIM or a SUMO motif, or both (Fig. 3D). Some known SUMOylated proteins such as PARP1 and RAN were also found in our list. The identified candidates included actin-binding proteins (such as Arp2), histone modifiers, nuclear matrix components (such as PARP1, RAN), endocytic vesicular transport proteins (ARF3, RAB1B, RAB7), translation regulator, enzyme regulatory proteins, antioxidant proteins. RAB7 and several members of the intracellular vesicular transport system being in the list was intriguing (Fig. 3D). The SCV extensively relies on the endocytic pathway and is known to interact with Rho GTPases and the Rab family proteins, a process required for stability of the SCV. From among the various identified proteins, since RAB7 assumes a central role in the endocytic pathway as well as S. Typhimurium biology, in the current study we focused on RAB7 in greater detail.
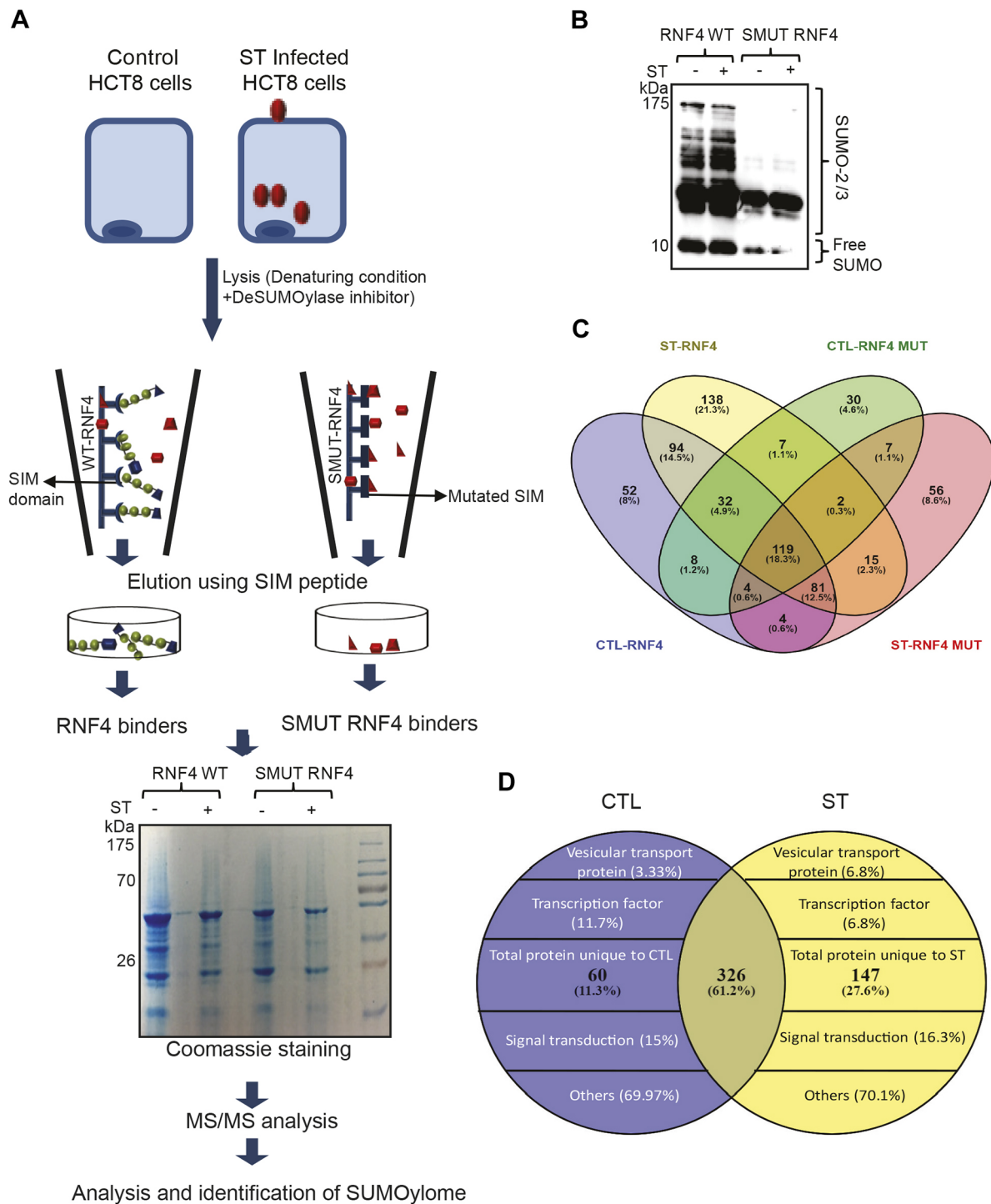
Fig. 2. *S*. Typhimurium infection leads to altered SUMO2/3 proteome. (A) Schematic representation of steps involved in SUMO2/3 proteome isolation by tandem mass spectrometry (MS/MS). HCT-8 cells infected with *S*. Typhimurium for 4 h were lysed and the SUMO2/3 proteome was enriched using purified RNF4 protein (RNF4 WT) as bait, or using the RNF4 SIM mutant (SMUT-RNF4) as a negative control. The bound proteome was eluted using buffer with an excess of SUMO-interacting motif (SIM) peptides. SDS-PAGE represents the pulldown samples from both RNF4 and RNF4 SIM mutant baits. Excised bands from the SDS-PAGE were used for in-gel digestion and processed for MS/MS analysis. Representative data obtained from three independent biological replicates is shown here. (B) Purified RNF4 and RNF4 SIM mutant fractions were also immunoblotted and probed with anti-SUMO2/3 antibody. (C) Venn diagram displaying individual proteins identified from control, *S*. Typhimurium-infected (ST) from RNF4 bait and the RNF4 SIM mutant (RNF4 MUT). (D) Venn diagram displaying number of unique SUMOylated proteins identified in control (CTL) and *S*. Typhimurium-infected (ST) samples that fall within the indicated function category.

RAB7 is SUMOylated at K175

Capture of RAB7 by RNF4 beads allowed us to examine the SUMO-modification of RAB7. We initially carried out immunoprecipitation

(IP) experiments with anti-SUMO2/3 antibodies followed by immunoblotting for RAB7. Although native RAB7 is a 24 kDa protein, we were able to detect several high molecular bands in the
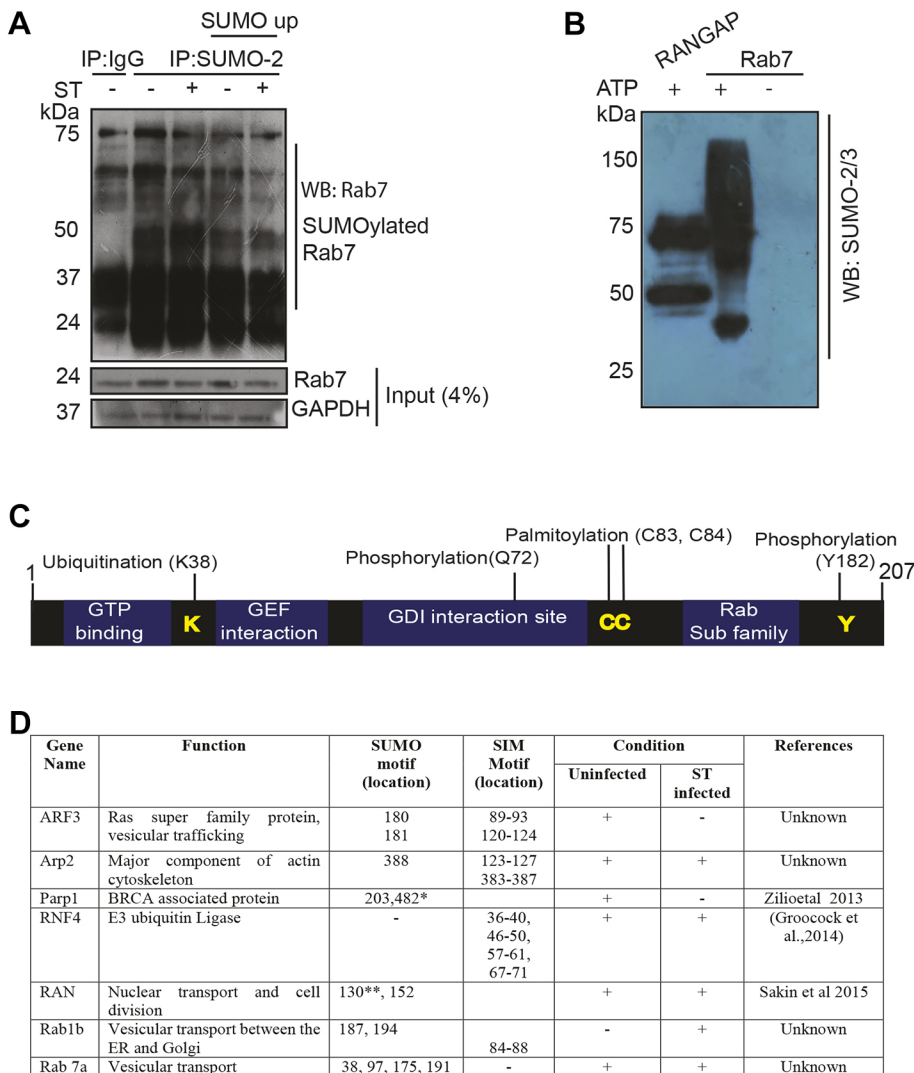
Fig. 3. RAB7 SUMOylation is inhibited during S. Typhimurium infection. (A) Control HCT-8 cells and those transfected with pcDNA/UBC9 were infected with S. Typhimurium for 4 h. The cells were lysed and immunoprecipitated (IP) with anti-SUMO2/3 antibodies followed by immunoblotting with anti-RAB7 antibodies (upper panel), or GAPDH (bottom panel). A portion of the original lysates was loaded as input (middle panel). (B) Purified fractions of RAB7 and RANGAP protein were subjected to *in vitro* SUMOylation assays in the presence (+) and absence (−) of ATP for 1 h. Subsequently, the mixture was loaded onto SDS-PAGE and immunoblotted with anti-SUMO2/3 antibodies. These are representative of data obtained from three independent experiments. (C) Schematic showing domain architecture of RAB7, highlighting regions of known post-translational modifications. (D) List of selected SUMO-modified protein identified by MS/MS analysis in control and S. Typhimurium infection (Zilioetal, 2013; Groocock at al., 2014; Sakin et al., 2015).

Gene Name	Function	SUMO motif (location)	SIM Motif (location)	Condition		References
				Uninfected	ST infected	
ARF3	Ras super family protein, vesicular trafficking	180 181	89-93 120-124	+	-	Unknown
Arp2	Major component of actin cytoskeleton	388	123-127 383-387	+	+	Unknown
Parp1	BRCA associated protein	203,482*		+	-	Zilioetal 2013
RNF4	E3 ubiquitin Ligase	-	36-40, 46-50, 57-61, 67-71	+	+	(Groocock et al.,2014)
RAN	Nuclear transport and cell division	130**, 152		+	+	Sakin et al 2015
Rab1b	Vesicular transport between the ER and Golgi	187, 194	84-88	-	+	Unknown
Rab 7a	Vesicular transport	38, 97, 175, 191	-	+	+	Unknown

immunoprecipitated samples (Fig. 3A). We reasoned that these bands may be chains of SUMO2/3 modification. Notably, SUMOylated RAB7 was more pronounced in control cells compared to *S.* Typhimurium-infected samples (Fig. 3A; Table S1). In samples where SUMOylation was upregulated by overexpressing UBC9, we observed slightly decreased RAB7 modification. We further subjected purified protein fractions of wild-type RAB7 to an *in vitro* SUMOylation assay (IVSA) performed in the presence of SUMO2/3. Briefly, 500 nM of purified RAB7 or RANGAP (positive control) was added to a reaction mixture containing SUMO2, E1 and E2 SUMO enzyme and in the presence and absence of ATP. RANGAP1 was used as a positive control (Gareau et al., 2012). After completion of the reaction, the mixture was run on SDS-PAGE and immunoblotted using anti-SUMO2/3 antibodies (Fig. 3B). We observed several bands that ran higher than the predicted molecular weight of RAB7, confirming SUMO-modification of RAB7. However, in the absence of ATP, we did not observe these higher mobility bands (Fig. 3B, lane 3). These and our earlier proteome data led us to conclude that RAB7 undergoes SUMOylation.

RAB7 full-length protein is known to undergo multiple modifications, each of which contributes to different RAB7 functions. As shown in Fig. 3C, the modifications involve ubiquitylation (K38), phosphorylation (Q72, Y182) and

palmitoylation (C83, C84). To determine the location of RAB7 SUMOylation, purified wild-type RAB7 was subjected to IVSA, then the mixture was resolved on SDS-PAGE. The entire lane from the gel was cut and processed for LC-MS/MS analysis (Fig. 4A). The spectrum of obtained proteins were identified using ChopNSpice software. For identification of SUMOylation sites with the Mascot search engine, all MS/MS spectra were searched against a new FASTA file that was created using ChopNSpice software. Briefly, the parameters that were included were a mass tolerance of 10 ppm in MS mode and 0.8 Da in MS/MS mode; zero missed cleavages. The analysis also included consideration of: (1) methionine oxidation and (2) cysteine carboxy-amidomethylation as variable modifications. All high abundance peaks had to be assigned to y- or b-ion series and were used for the determination of potential sites of modification. We identified 13 potential SUMO sites (Table S2) from this analysis. But from these sites, we narrowed the candidates for further investigation down to K38, K97 and K175 based on either high confidence score (>95% score) or high score based on *in silico* SUMO-motif search analysis. To validate the above findings, we performed site-directed mutagenesis of each of these lysine residues to arginine (K38R, K97R and K175R) and purified the mutant proteins from *E. coli*. The purified variants of RAB7 (WT RAB7, RAB7^{K38R}, RAB7^{K97R} and RAB7^{K175R}) were subjected to an *in vitro* SUMOylation assay.
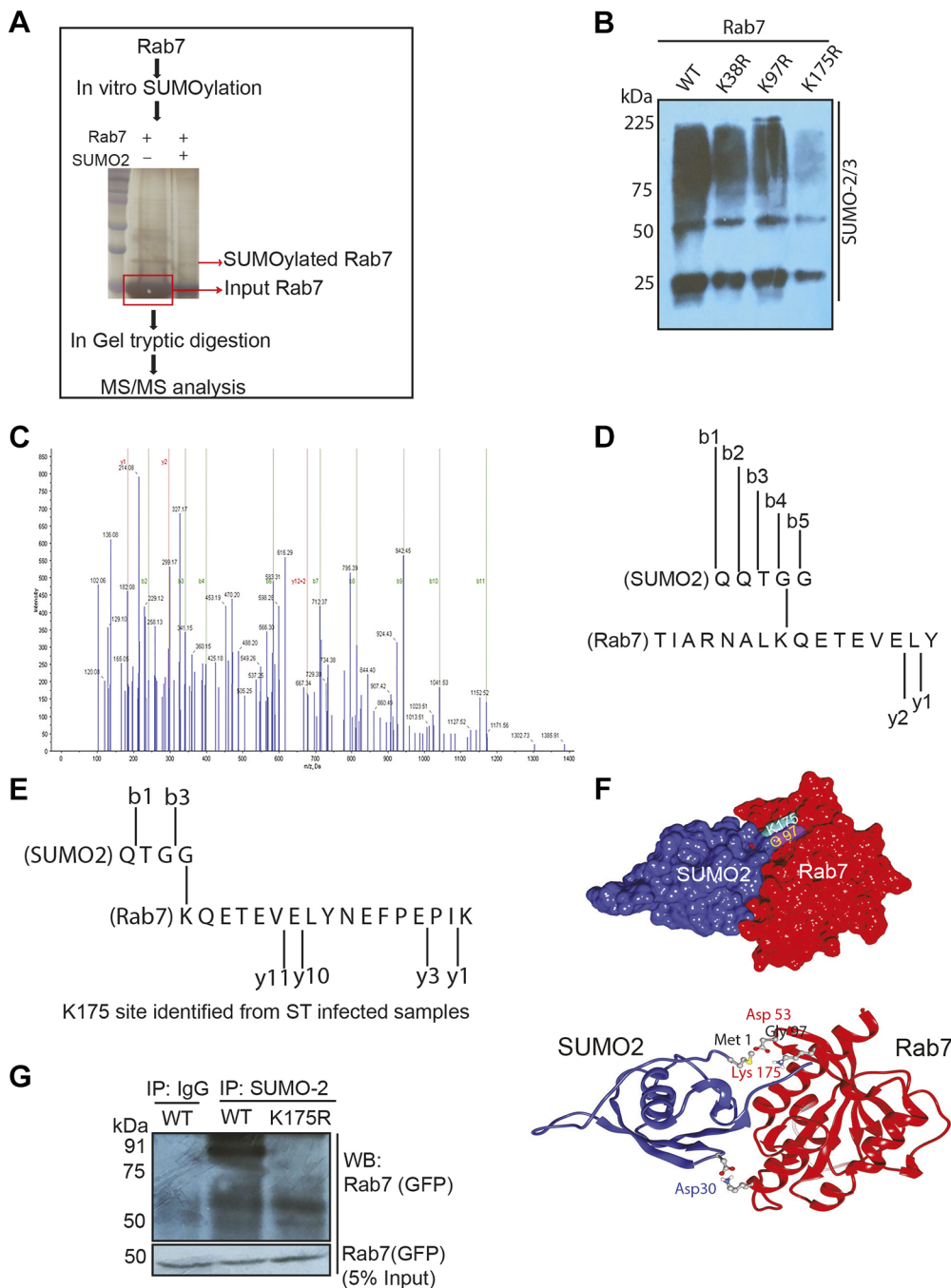
Fig. 4. RAB7 undergoes SUMO modification at lysine 175.
(A) Schematic representation of steps involved in MS/MS analysis of identification RAB7 SUMOylation site. Protein bands representing native RAB7 and SUMOylated RAB7 are highlighted (with arrows) in the silver-stained gel. (B) Immunoblot representing the *in vitro* SUMOylation of purified WT RAB7, RAB7^{K38R}, RAB7^{K97R} and RAB7^{K175R} mutants. (C,D) The MS/MS spectra representing RAB7^{K175R} SUMOylation (C) and the corresponding amino acids identified from the spectra (D). The spectrum represents a precursor molecular weight of 1463.7±0.8; confidence, 96%. (E) HCT-8 cells infected with *S.* Typhimurium were lysed and samples were run on an SDS-PAGE followed by tandem MS/MS (as described in D). The amino acids corresponding to the actual SUMOylation site in RAB7 and SUMO2/3 as identified are represented in the figure. (F) Computational molecular docking of available protein structures of SUMO2 and RAB7 from PDB to check their interaction using ClusPro program. Upper panel: 3D structure of SUMO2/3 (blue) and RAB7 (red), Lower panel: ribbon structure of SUMO2/3 and RAB7. The juxtaposed C-terminal G97 (Gly 97) residue of SUMO2/3 and the K175 (Lys 175) residue of RAB7 are represented. (G) Cells transfected with either wild-type GFP-tagged RAB7 (WT) or GFP-tagged mutant RAB7^{K175R} were infected with *S.* Typhimurium for 4 h, were lysed, immunoprecipitated for SUMO2/3 and immunoblotted with anti-GFP antibody to identify GFP-tagged WT RAB7 and RAB7^{K175R}). A portion of the original lysates was loaded as input (lower panel). The data shown here are representative from three independent experiments.

As can be seen in Fig. 4B, WT RAB7 displayed SUMOylation in the presence of ATP, so did mutants RAB7^{K38R} and RAB7^{K97R}. We observed that SUMOylation was almost completely abolished in the case of the K175R mutant, indicating that this residue may be the site of SUMO modification. We reanalysed the MS/MS data to specifically look at the signatures of K175 SUMO modification. In line with these assumptions, we were able to detect y and b ions RAB7 and SUMO2 in the precise K175 location (Fig. 4C,D). To further confirm these findings, we reverted back to our decoy database that was generated using all possible combinations of RAB7 SUMOylation. This was based on every possible lysine that could potentially undergo a SUMO modification. Based on this, a theoretical database (FASTA form) was generated. This database was searched against the actual spectrum of peptides obtained from

MS/MS complex proteomic analysis (described in Fig. 4C) using the ChopNSpice approach. Interestingly, we were able to see the signatures of K175 modification (Fig. 4E).

To discern the site of RAB7 SUMOylation in greater detail, we carried out an *in-silico* docking experiment between SUMO2 (PDB ID: 5GHC) and RAB7 (PDB ID: 3LAW) structures available in the PDB database. In our analysis, several important aspects connected to RAB7 SUMOylation were considered, including, but not restricted to: (1) RAB7 and SUMO2/3 supramolecular geometry, (2) availability of lysine for isopeptide bond formation and (3) minimal energy scores for the interactions. Using the data, we inferred potential interaction between RAB7 and SUMO2 at three positions, namely K38, K97 and K175 of RAB7 with G97 of SUMO2 (Fig. S2). Further, by also including molecular docking,

K175 of RAB7 was selected. The analysis revealed the interaction between RAB7 and SUMO2/3 to be very compact (Fig. 4F). In the docked model, the C-terminal of SUMO2 places itself within the reach of experimentally validated K175. Both the partners appear to form a steady complex, stabilized by 11 hydrogen bonds and salt bridges between the D30 [outer domain (OD)1 and OD2] and M1 (amide N of the N-terminus) residues of SUMO2 and the K137 (NZ domain) and D53 (OD1) residues of RAB7. In complex, both the proteins have a buried interface area of 852 Å.

In addition, immunoprecipation using antibodies against SUMO2/3, followed by immunoblotting for RAB7 using anti-GFP antibodies, yielded prominent bands in results from cells transfected with WT RAB7 but not with those transfected with the RAB7^{K175R} mutant (Fig. 4G). Taken together, these data revealed that RAB7 undergoes SUMOylation and the K175 position is the predominant site.

SUMOylation of RAB7 modulates its stability

We next set out to understand the potential connection between SUMO-modification of RAB7 and its function, particularly in the context of S. Typhimurium infection. The possible ways by which SUMOylation is capable of changing the fate of a modified protein are by changing its: (1) stability or half-life, (2) capacity to interact with other proteins and (3) activity. To test these possibilities in RAB7, the SUMOylation machinery of HCT-8 cells was transiently activated, as done previously, by overexpressing genes encoding proteins of the SUMOylation pathway. Expression of RAB7 and some protein members of the VTP were examined. In uninfected cells, overexpression of any of the SUMOylation machinery components resulted in no major change in levels of early endosomal protein, EEA1or lysosomal glycoprotein, LAMP1 (Fig. S3C). However, a significant reduction in the expression of RAB7 was observed in case of cells with upregulated UBC9 (Fig. 5A, B). While S. Typhimurium infection resulted in an increase in EEA1 and RAB7 protein levels in SUMOylation control cells, activation of SUMOylation resulted in reduction of RAB7 protein levels (Fig. 5A, B). Taken together these results led us to conclude that upregulation of SUMOylation machinery, particularly of UBC9, adversely affects RAB7 protein expression both in uninfected and infected cells. Further, we used a siRNA-mediated knockdown of RAB7 (Fig. S3A) and examined the number of CFUs of S. Typhimurium (Fig. S3B). We saw that lowering of RAB7 expression had a direct effect on S. Typhimurium intracellular multiplication. Literature suggests that inactive RAB7 is typically dispersed uniformly in the cytoplasm, while upon activation it is recruited to the membranes of endosomes or phagosomes (Soldati et al., 1995). Subcellular distribution of Rab7 is indicative of its active (GTP bound) and inactive (GDP bound) forms that, in turn, can affect Salmonella CFU and other relevant functions of RAB7.

Since RAB7 protein levels were regulated by cellular SUMOylation status, we reasoned that SUMOylation may influence the stability of RAB7. To test this, using protein synthesis inhibitor cycloheximide, we blocked the de novo synthesis of RAB7. Thus, under conditions where no new RAB7 can be synthesized, we monitored the kinetics of its existing copies in SUMOylation activated and infected cells. It was evident that, in the absence of any fresh synthesis, the existing levels of RAB7 slowly diminished due to degradation. In SUMOylation activated conditions, the levels of RAB7 diminished faster compared to untreated controls, indicating that SUMOylation-dependent reduction of RAB7 protein levels was due to its degradation (Fig. 5C,D). Based on this, the approximate time for the level of

RAB7 to reach 50% of its original was calculated (Fig. 5E). We were able to discern that in SUMO-activated cells the half-life of RAB7 was shorter (5.6 h) than in untreated cells (7.5 h). We thus hypothesized that RAB7 turnover is SUMOylation dependent.

To further corroborate this hypothesis, we inhibited the ubiquitin-dependent proteasome degradation machinery using MG132 (a proteasome inhibitor), and examined the effect on RAB7 protein levels. We observed that MG132 treatment was able to rescue RAB7 degradation in SUMO-activated conditions. This indicated that SUMOylation-mediated RAB7 turnover was via the proteasome machinery (Fig. 5F,G). The proteasome pathway relies on ubiquitylation before the target protein can undergo degradation. Immunoprecipitation using anti-ubiquitin antibodies followed by RAB7 immunoblotting yielded RAB7 bands of higher molecular weight, revealing ubiquitin modification (Fig. S3D). A subtle increase in RAB7 ubiquitylation in S. Typhimurium infected samples was also seen, while samples subjected to both SUMO upregulation and infection showed much more pronounced ubiquitylation (Fig. S3E). Taken together, these data revealed that SUMO activation results in a shortened half-life of RAB7 and, both in resting cells and infected cells, RAB7 turnover occurs via the ubiquitin-dependent proteasome pathway.

SUMOylation of RAB7 prevents bacterial multiplication and SCV stability

We next delved deeper into the significance of the altered stability of RAB7 through SUMOylation on Salmonella biology. We overexpressed either WT RAB7 or SUMOylation-deficient mutant RAB7^{K175R} in HeLa cells followed by S. Typhimurium infection, and then performed imaging by confocal microscopy (Fig. 6A). S. Typhimurium was imaged by labelling encoded plasmids with mCherry (red), and RAB7 was labelled with a GFP tag (imaged as pseudocolour magenta). Co-localization of RAB7 with S. Typhimurium was then scored (Fig. 6B). Surprisingly, the number of S. Typhimurium–RAB7 co-localisation spots was significantly higher in cells transfected with RAB7^{K175R} compared to cells expressing WT RAB7. Quantification of fluorescence levels revealed a more pronounced interaction between RAB7 and S. Typhimurium where the RAB7^{K175R} mutant was expressed, compared to WT RAB7 (Fig. 6A,B). To see if RAB7^{K175R} also displayed other features relevant to S. Typhimurium infection, we tested its interaction with RILP by immunoprecipitation. S. Typhimurium is known to inhibit the RAB7–RILP interaction. In line with our previous results, lysates from S. Typhimurium-infected cells expressing WT RAB7 and RAB7^{K175R} showed interaction when immunoprecipitated and probed with antibodies against RILP. However, this interaction was stronger in the case of WT RAB7 compared to the RAB7^{K175R} mutant, indicating that knocking down the SUMOylation of RAB7 at K175 was deleterious to its interaction with its cognate partner RILP (Fig. 6C). It has previously been shown that unlike the interaction between RAB7 and RILP, the interaction between RAB7 and PLEKHM1 is beneficial to S. Typhimurium infection through stabilisation of the SCV (McEwan et al., 2015). To explore the mechanism by which SUMOylation of RAB7 might alter SCV biogenesis or stability, we investigated the effect of SUMOylation on the interaction between RAB7 and PLEKHM1. We observed that PLEKHM1 co-immunoprecipitated with WT RAB7; however, the interaction was much more pronounced in cells expressing RAB7^{K175R} (Fig. 6D). Further, we carried out a flow cytometry analysis to understand the interaction between RAB7 and PLEKHM1 in the context of RAB7 SUMOylation. HCT-8 cells
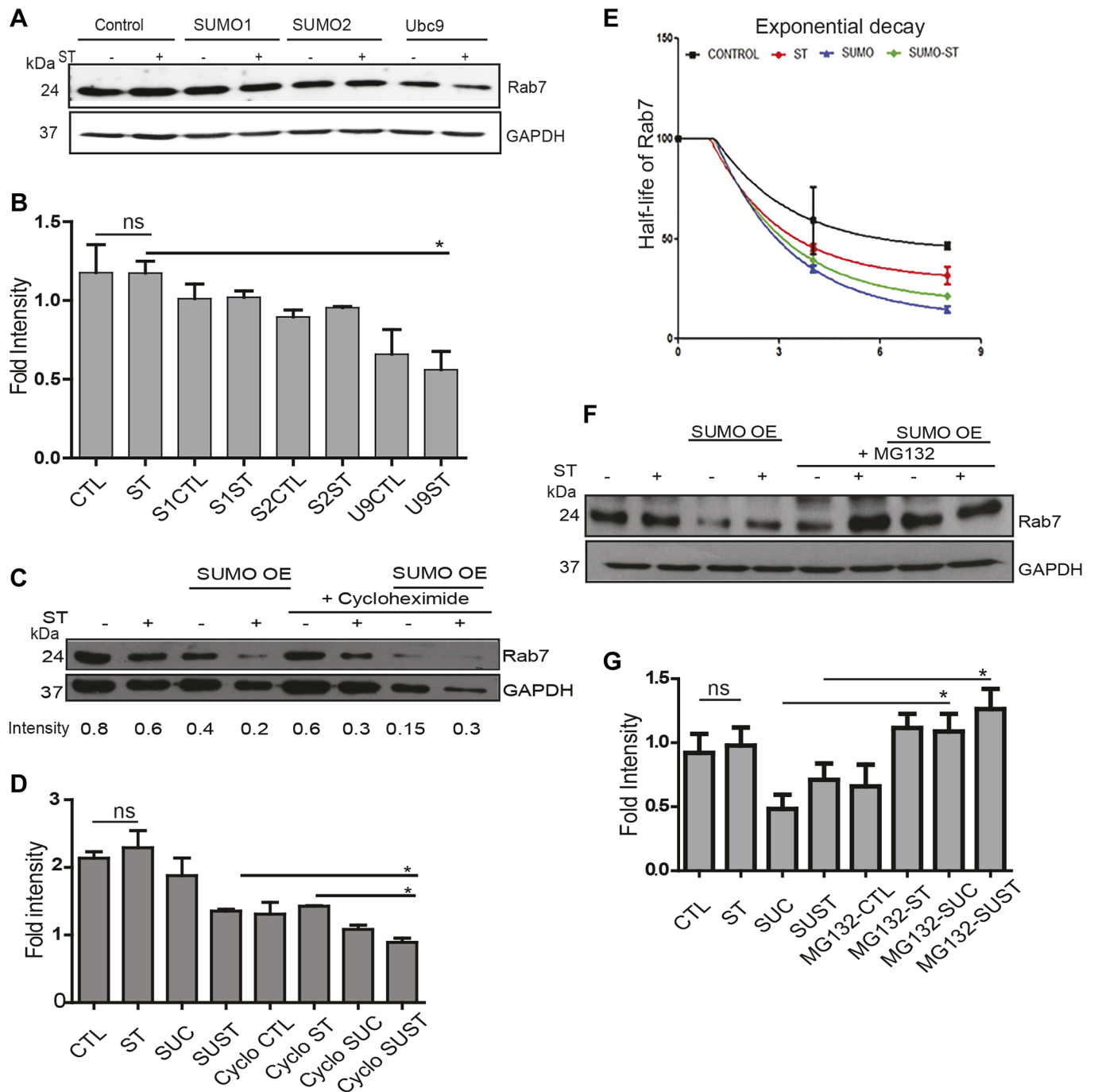
Fig. 5. RAB7 expression and stability depends upon SUMOylation pathway. (A) HCT-8 cells were transfected with pEYFP SUMO1, pcDNA HA-SUMO2 or pcDNA/UBC9 constructs 24 h prior to *S.* Typhimurium infection for 4 h. The lysates were immunoblotted for RAB7 (upper panel) and GAPDH (lower panel). (B) Mean±s.e.m. fold-change in densitometric values (from three independent experiments) of the bands in A were calculated, normalized to GAPDH and plotted. CTL, control; ST, *S.* Typhimurium-infected; S1, SUMO1; S2, SUMO2; U9, UBC9. (C) pcDNA/UBC9-transfected HCT-8 cells treated with or without 20 µM of cycloheximide 1 h before and throughout the *S.* Typhimurium infection were immunoblotted for RAB7 and GAPDH. The 'intensity' values give the densitometry of the represented bands. SUMO OE, SUMO-overexpressed. (D) Mean±s.e.m. fold-change in densitometric values (from three independent experiments) of the bands in C were calculated, normalized to GAPDH and plotted. SUC, SUMO-activated control; SUST, SUMO-activated plus *S.* Typhimurium-infected; Cyclo, cycloheximide treated. (E) Half-life of RAB7 was calculated from the blots of cycloheximide-treated samples in C, calculating the decay curves plotted against time. (F) pcDNA/UBC9-transfected HCT-8 cells treated with and without 20 µM of MG132 for last 2 h of *S.* Typhimurium infection were immunoblotted for RAB7 and GAPDH. (G) Mean±s.e.m. fold-change in densitometric values (from three independent experiments) of the bands in F were calculated, normalized to GAPDH and plotted. *$P \leq 0.05$; ns, not significant by unpaired Student's *t*-test.

were transfected with plasmids encoding DsRed–PLEKHM1 and either GFP-labelled WT RAB7 or GFP-labelled RAB7^{K175R}. The cells were then infected with *S.* Typhimurium and prepared for flow cytometry. The results were gated for cells expressing GFP and

the percentage of cells also expressing DsRed–PLEKHM1 was analysed. We saw that in cells expressing WT RAB7, the percentage of PLEKHM1 co-expression upon *S.* Typhimurium infection was 12.9%, while in cells expressing RAB7^{K175R}, the level of
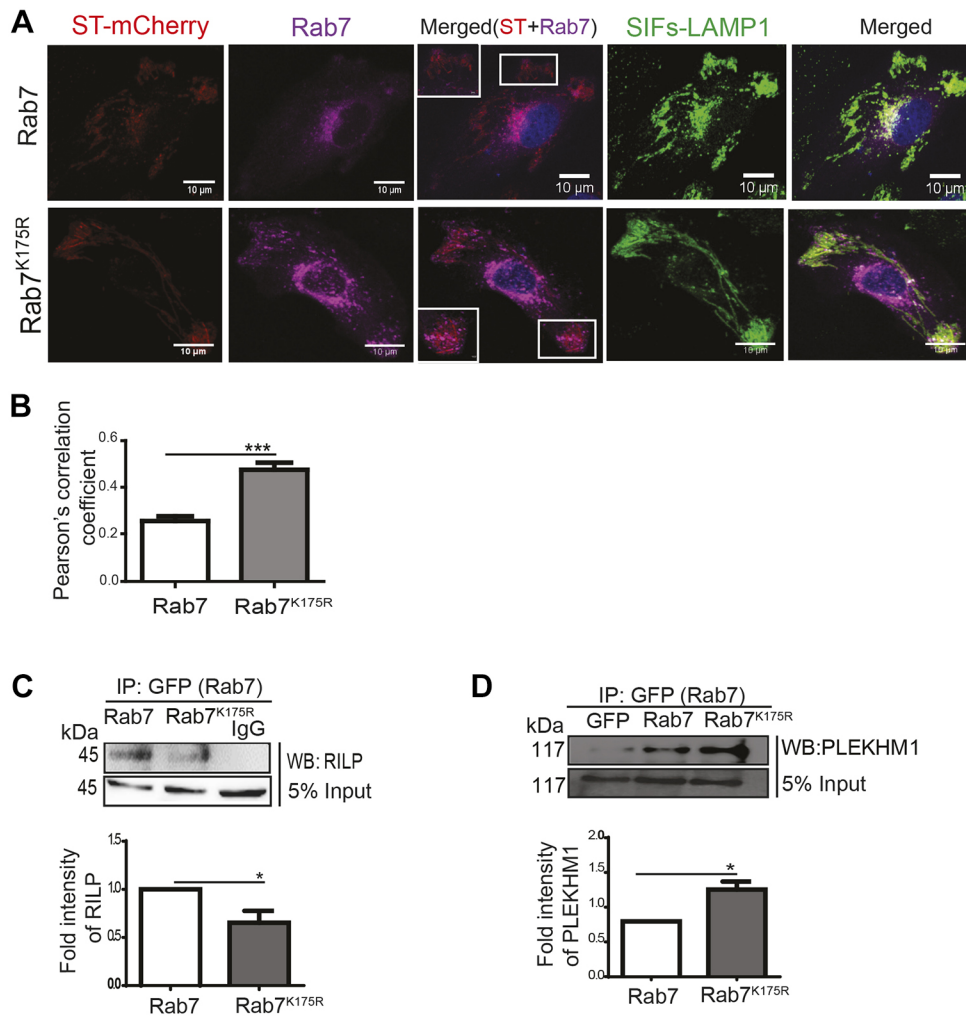
Fig. 6. RAB7 SUMOylation affects its interaction with RILP and PLEKHM1. (A) Confocal images showing the co-localization of RAB7 (magenta) or RAB7^{K175R} (magenta) with *S.* Typhimurium (red) in HeLa cells infected for 16 h. The intracellular filament formation (SIFs) was visualized by LAMP1 staining (green). Scale bars: 10 μm. (B) The co-localization of RAB7 and *S.* Typhimurium was quantified by Pearson's correlation from five independent experiments. Representative areas used for quantification are highlighted in A (rectangle in merged panels). Mean±s.e.m. from three independent experiments were plotted. (C) Immunoblot representing the interaction between RILP–GFP and RAB7 or RAB7^{K175R} from HCT-8 cells infected for 4 h with *S.* Typhimurium, immunoprecipitated using anti-GFP antibody and probed with anti-RILP antibody, with anti-rabbit IgG as control. A portion of the input sample was loaded and probed with anti-RILP antibody (bottom panel). The graph represents mean±s.e.m. fold-change in densitometric values of RILP, showing the interaction of RILP with RAB7^{K175R}, normalized to RAB7. (D) Immunoblot representing the interaction between PLEKHM1 and RAB7 or RAB7^{K175R}. Cells transfected with GFP (mock plasmid), RAB7–GFP or RAB7^{K175R} were infected for 4 h with *S.* Typhimurium were lysed and immunoprecipitated using anti-GFP antibodies and probed with anti-PLEKHM1 antibody (upper panel). A portion of the input sample was loaded and probed with anti-PLEKHM1 antibody (bottom panel). The data shown here are representative of three independent experiments. The graph represents mean±s.e.m. fold-change in densitometric value of PLEKHM1, showing the interaction of PLEKHM1 with RAB7^{K175R}, normalized to RAB7. *$P \leq 0.05$, ***$P \leq 0.001$ by unpaired Student's *t*-test.

co-expression was 18.04%. We concluded that SUMO-deficient RAB7^{K175R} enabled these cells stabilise PLEKHM1 and thereby enhanced the possibility of interaction between RAB7 and PLEKHM1 (Fig. S4A,B). We next went on to check the dynamics of PLEKHM1 under *S.* Typhimurium infection conditions. We observed that the recruitment of PLEKHM1 increased at 7 hpi in cells expressing the RAB7^{K175R} mutant. Moreover, there was a higher level of co-localization of RAB7^{K175R} and PLEKHM1 at this time point compared to WT RAB7 and PLEKHM1 (Fig. S4C). Taken together, these data suggest that a non-SUMOylatable RAB7^{K175R} mutant interacts more strongly with PLEKHM1 and is beneficial for intracellular survival of *S.* Typhimurium.

The localization of RAB7 is a prerequisite for its function, active GTP-bound RAB7 is always a membrane resident. Cells were made

to express either GFP-tagged WT RAB7 (GFP–WT-RAB7) or GFP-tagged RAB7^{K175R} (GFP–RAB7^{K175R}) (Fig. 7A), so that separate bands of ectopic protein could be visualised in immunoblots. To check if inhibition of RAB7 SUMOylation affected its localization, we fractionated membrane and cytoplasmic constituents of uninfected and infected cells. A portion of GFP–WT-RAB7 displayed membrane localization, showing the presence of the active form of the protein. Between infected and control samples, WT RAB7 band intensity was more or less equal (Fig. 7A). Contrary to this, cells expressing GFP–RAB7^{K175R} displayed a clear increase in the amount of the membrane-resident form of the protein. These data indicated that RAB7^{K175R}, which is unable to undergo SUMOylation, was capable of reaching the membrane.

During infection, it is known that a portion of *S.* Typhimurium usually resides in the cytosol of the host cell. To examine if RAB7
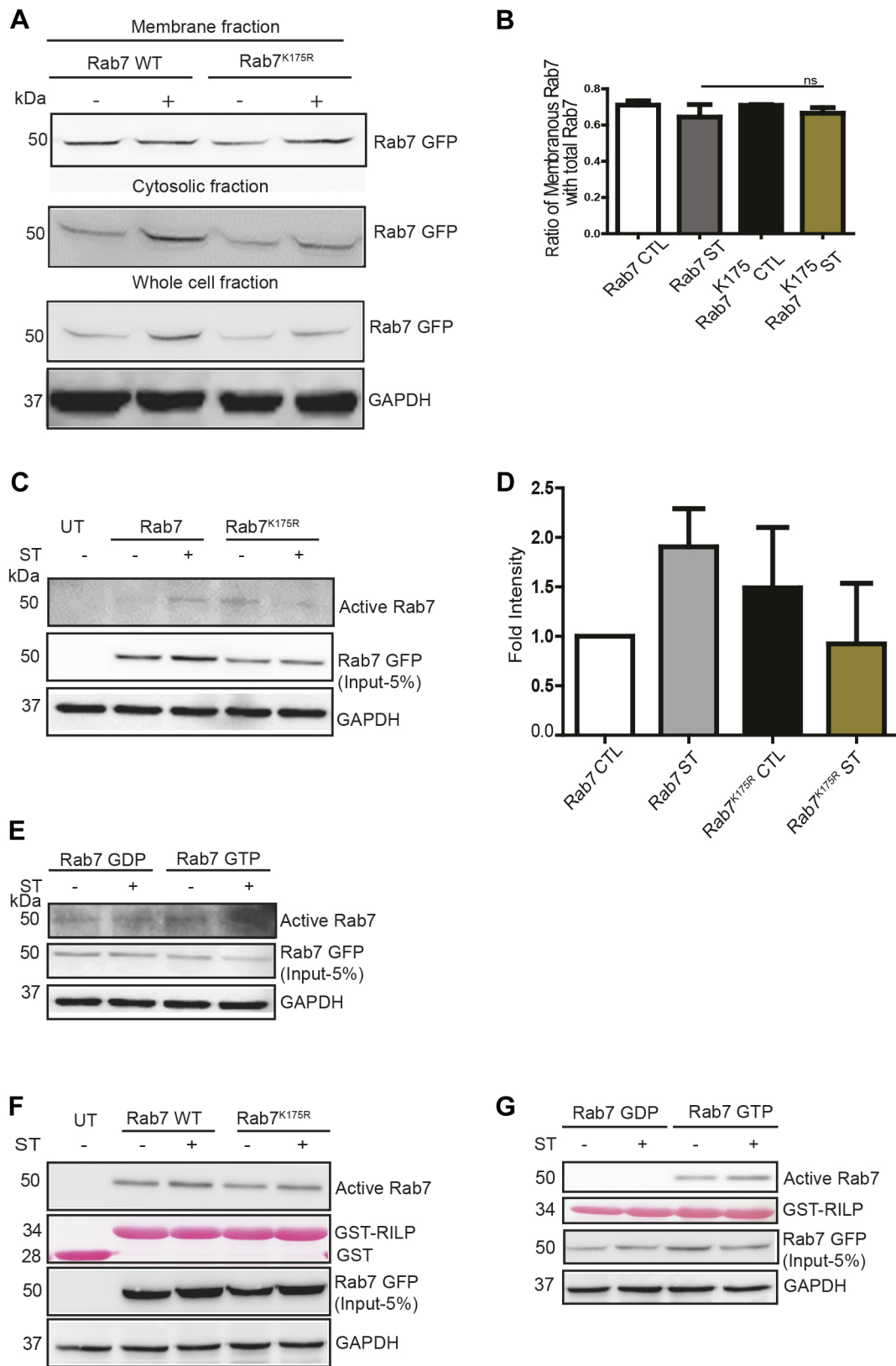
Fig. 7. See next page for legend.

SUMOylation plays a role in this subcellular distribution of bacteria, we checked the localization of SUMOylated and SUMO-deficient RAB7 in the cytosol and the vacuole. The percentage of LAMP1-positive *S.* Typhimurium (vacuolar pool of *S.* Typhimurium) in

comparison to the total number of intracellular bacteria was quantified. The data revealed that amount of LAMP1-positive *S.* Typhimurium was higher in cells expressing RAB7[K175R] (Fig. S5A,B) compared to those expressing WT RAB7. Similarly,

Fig. 7. SUMOylation of RAB7 increases its GTPase activity. (A) HCT-8 cells were transfected with plasmids encoding GFP–RAB7 and GFP–RAB7^{K175R}. Cells were infected with S. Typhimurium for 7 h, followed by preparation of cytosolic and membrane fractions. Equal amounts of protein lysates were loaded onto SDS-PAGE gels and probed with anti-RAB7 antibody (upper panel). Similarly, whole cell fractions were prepared and probed with anti-RAB7 (GFP–RAB7) and anti-GAPDH (lower panel) antibodies. (B) The graph plotted from the mean±s.e.m. densitometric values of the bands in A, giving the ratio of protein in membrane fraction compared to total protein samples. CTL, control; ST, S. Typhimurium-infected; ns, not significant. (C) HCT-8 cells were transfected with plasmids expressing RAB7 and RAB7^{K175R}, then infected with S. Typhimurium for 7 h. The samples were lysed and immunoprecipitated with antibodies specific for active RAB7 and probed with anti-RAB7 (polyclonal antibody, described in methodology). (D) Mean±s.e.m. fold-change in densitometric values of the bands in C were calculated, normalized to GAPDH and plotted. (E) HCT-8 cells were transfected with plasmids expressing RAB7 GDP-locked (RAB7^{T22N}) and RAB7 GTP-locked (RAB7^{Q67R}), then infected with S. Typhimurium for 7 h. The samples were lysed and immunoprecipitated with antibodies specific for active RAB7 and probed with anti-RAB7 antibody. The data shown here are representative of from three independent experiments. (F,G) HCT-8 cells were transfected with indicated plasmid constructs and infected with S. Typhimurium for 7 h. Active RAB7 was pulled down by GST–RILP and detected with anti-RAB7 antibody. The expression of GST–RILP and GST were detected by Ponceau S staining. 5% input is shown for the different transfected RAB7–GFP plasmids. GST was used as a loading control in F, GAPDH was used as a loading control in F,G.

we quantified the amount of LAMP1-negative S. Typhimurium (cytosolic bacteria) through visual observation of microscopic images. Cells expressing RAB7^{K175R} displayed fewer cytosolic bacteria compared to WT RAB7-transfected cells (Fig. S5C). This indicated that non-SUMOylatable RAB7 was functionally inactive and its presence was beneficial for S. Typhimurium infection. To further probe this aspect, cells were transfected with plasmids encoding a GDP-locked form of RAB7 (GFP–RAB7-GDP), a GTP-locked form of RAB7 (GFP–RAB7-GTP), and GFP–WT-RAB7 or GFP–RAB7^{K175R}. These cells, along with untransfected cells, were infected with S. Typhimurium. Cells lysates were subjected to immunoprecipitation with antibodies specific for the active form of RAB7. We observed that in GFP–WT-RAB7-expressing cells, upon infection, the active form displayed a discernible increase (Fig. 7C,D). In contrast to this, in GFP–RAB7^{K175R}-expressing cells, the levels of active form of RAB7 appeared to diminish. In uninfected cells, however, the GFP–RAB7^{K175R}-expressing cells seemed to contain more active RAB7 compared to the infected cells. Cells expressing GTP-locked RAB7 showed the presence of the active form in both uninfected and infected cells while, as expected, those expressing the GDP-locked form displayed lower levels of active RAB7 (Fig. 7E). To further corroborate this finding, we overexpressed the plasmids encoding GFP–WT-RAB7 or GFP–RAB7^{K175R} in HCT-8 cells, followed by infection with S. Typhimurium for 7 h. The active form of RAB7 was pulled down using the Rab-binding domain of GST–RILP, followed by immunoblotting for RAB7. We observed that on S. Typhimurium infection, the amount of active RAB7 was reduced in cells expressing the SUMO mutant GFP–RAB7^{K175R} compared to WT RAB7 (Fig. 7F). Cells expressing the GTP-locked form of RAB7 showed binding with GST–RILP, while those expressing GDP-locked RAB7 showed no interaction with GST–RILP, suggesting that the assay had worked properly (Fig. 7G). Taken together this data further supports the notion that in the absence of SUMOylation, RAB7 localization is not changed, but its activity is reduced.

Next, to examine the aspect of S. Typhimurium intracellular life governed by RAB7 SUMOylation, we looked at the stability of the SCV by scoring for SIFs (LAMP1-containing filaments). This was

analysed by visualising RAB7 (purple) and LAMP1 (green for SIFs) in infected cells. The presence of S. Typhimurium within the SCV was probed by DAPI staining. Infected cells expressing WT RAB7 displayed SIFs as expected. However, infected cells expressing RAB7^{K175R} displayed a significantly higher number of SIFs (Fig. 8A,B). The increase was almost 60%, revealing that the lack of SUMOylation at RAB7 K175 was beneficial to SIF formation. Considering the importance of SIFs in SCV maintenance, we next examined S. Typhimurium entry and intracellular multiplication, using a gentamycin protection assay. The CFUs were assayed at 2 hpi and 16 hpi in various samples. In line with the previous results, fold-change in bacterial multiplication between 16 hpi and 2 hpi was significantly higher in cells expressing RAB7^{K175R} compared to cells expressing WT RAB7 (Fig. 8C). Thus, we concluded that the presence of RAB7^{K175R} allowed better SIF formation, which in turn is beneficial for SCV maintenance and bacterial multiplication. The possibility of a dominant-negative function of RAB7^{K175R} can, therefore, not be ruled out.

Upon SUMO2/3 upregulation, we observed reduced bacterial multiplication and SIF formation. However, a recovery in bacterial multiplication and SIF formation was observed when the SUMO mutant RAB7^{K175R} was overexpressed in epithelial cells. To understand the connection, we co-transfected cells with plasmids encoding HA–SUMO2/3 (yellow) along with GFP–RAB7 or GFP–RAB7^{K175R} (magenta). These cells were infected with mCherry-labelled S. Typhimurium (red) for 16 h. The cells were then fixed and stained for LAMP1 to enumerate number of SIFs (green) along with the bacteria load (Fig. S6A). Based on the bacteria load in each cell, the infected cells were categorized into following three categories: <5 bacteria per cell (low bacterial load), 5–20 bacteria per cell (medium bacterial load) and >20 bacteria per cell (high bacterial load). In each category, the data was scored as a percentage against total infected cells. The analysis revealed that the percentage of cells with a high bacterial load was less in the case of SUMO2/3 overexpression (51%). However, in cells overexpressing RAB7^{K175R} alone, the percentage of cells with a high bacterial load was ∼67%, compared to ∼57% in cells overexpressing RAB7. The percentage of cells having high bacterial load in cells co-expressing WT RAB7 along with SUMO2 was ∼47% cells. Interestingly, co-expression of SUMO2 along with RAB7^{K175R} showed a significantly higher number (∼69%) of cells with a high bacterial load (Fig. S6B). These data suggest that non-SUMOylatable RAB7^{K175R} is able to overcome the negative effect of SUMO2/3 overexpression on S. Typhimurium infection.

To further confirm the above findings, the number of SIFs were quantified from the images obtained in the above experiment. The analysis revealed that the percentage of cells containing SIFs was reduced in cells transfected with plasmids encoding SUMO2/3 (∼34%) compared to those transfected with vector control (∼46%). Furthermore, the percentage of cells containing SIFs increased substantially upon overexpression of RAB7^{K175R} (∼49%) compared to overexpression of RAB7 (∼33%). Cells overexpressing SUMO2 and RAB7^{K175R} showed significantly increased SIF formation (∼59%) in comparison to those expressing SUMO2 and WT RAB7 (∼35%) (Fig. S6C). Overall, these findings suggest that by preventing the SUMOylation of RAB7, S. Typhimurium ensures better intracellular multiplication and SIF formation.

DISCUSSION

In the present work, we have probed the role of SUMOylation, a PTM pathway, in the intracellular life of S. Typhimurium. Our work
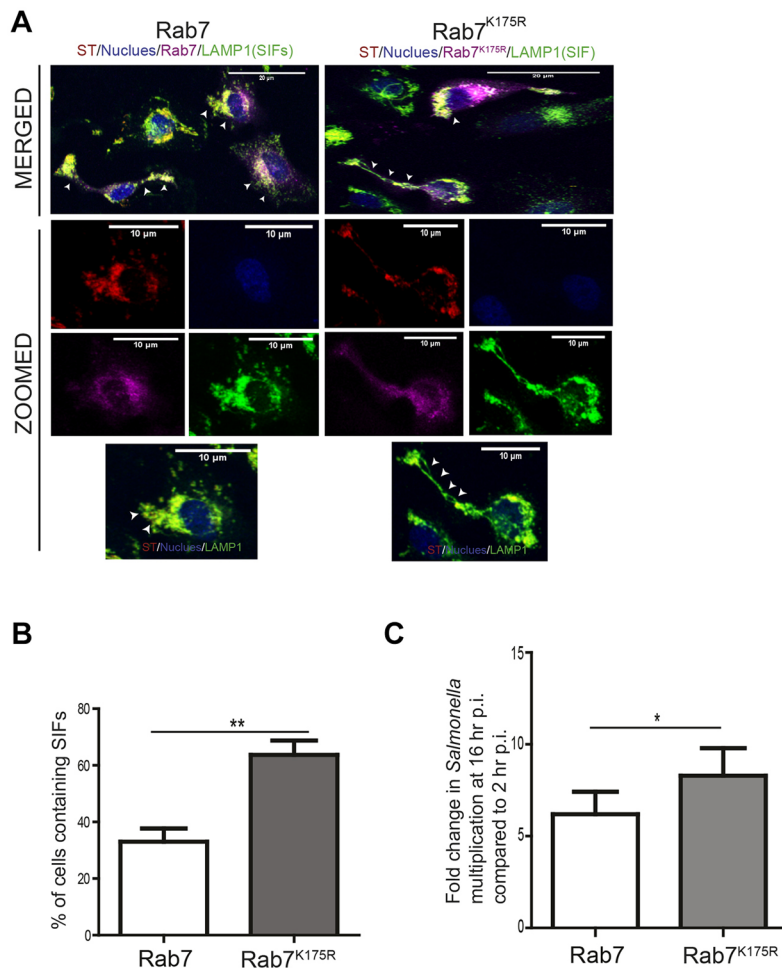
Fig. 8. RAB7 SUMOylation prevents SIF formation and intracellular multiplication of *S*. Typhimurium. (A) Cells transfected with plasmids encoding RAB7 or RAB7^{K175R} were infected with *S*. Typhimurium. Confocal images showing the status of intracellular filament formation (SIF, green), with cells overexpressing WT RAB7 or RAB7^{K175R} (magenta) and stained with LAMP1 (green) to enumerate SIFs (white arrows). Intracellular *S*. Typhimurium (red) after 16 h of infection was also imaged. Scale bars: 20 µm. (B) The graph represents the mean±s.e.m. of SIFs as obtained from confocal images. (C) A gentamicin protection assay was performed on HCT-8 cells infected for 2 h or 16 h. CFUs were used to calculate and plot mean±s.e.m. relative fold-change in bacterial multiplication. *$P \leq 0.05$, **$P \leq 0.01$ by Student's *t*-test.

has revealed an unexpected SUMO-modification of RAB7 that is blocked by *S*. Typhimurium as it was detrimental to several important aspects related to the intracellular life of the bacterium. We initially observed that any experimental upregulation of SUMOylation in cells led to a compromised infection, an effect that was slightly more pronounced when SUMO2/3 expression levels were manipulated. SUMO2/3, in contrast to SUMO1, is predominantly involved in conditions of cellular stress, including heat shock and DNA repair stresses (Domingues et al., 2015; Hendriks et al., 2015). A comprehensive proteomic analysis of *Listeria monocytogens*-infected HeLa cells revealed involvement of both SUMO1 and SUMO2/3 (Ribet et al., 2010). SUMOylome alteration, particularly the SUMO2/3 modified proteome, has been studied in the context of infection with herpes simplex virus (HSV-1) and influenza virus (Sloan et al., 2015). In light of this information, we looked at the SUMO2/3-modified proteome of *Salmonella*-infected cells. Clearly, we saw that a large fraction of the cellular proteome displayed a changed SUMO2/3 modification pattern, with altered proteins including translation regulators, enzyme regulatory proteins, antioxidant proteins, signalling molecules, immune mediators and vesicular transport proteins. Interestingly, there are proteins that selectively undergo SUMOylation during *S*. Typhimurium infection, which reveals that the overall downregulation of SUMOylation during infection is only a quantitative impression of the SUMOylome. These changes may be a combinatorial effect mediated by *S*. Typhimurium or a host

response to the infection. Among the altered proteins, VTP members were of particular interest, since the *S*. Typhimurium intracellular life largely relies on the components of this machinery. Through the whole process of infection, SCV generation and maintenance, there are ~18 different GTPases that are involved in different stages. Thus, the GTPases are integral to the intracellular life of *S*. Typhimurium. For a successful infection, *S*. Typhimurium interferes with several GTPases of the host such as Rab32, which has been shown to be cleaved by cysteine protease GtgE of *S*. Typhimurium (Wachtel et al., 2018). Among these, RAB7 occupies a central role, participating in a plethora of different cellular activities including late endosome maturation, lysosomal fusion, autophagy and SCV maintenance (Jordens et al., 2001; Vanlandingham and Ceresa, 2009; Girard et al., 2014). Understandably, such diverse activities may require fine tuning by multiple regulatory mechanisms. Prenylation, phosphorylation, ubiquitylation and palmitoylation are post-translational modifications that are known to affect RAB7. In addition availability of GTP/GDP and interaction with discrete sets of interacting partners at different situations are examples of regulatory modes for RAB7 (Wu et al., 2009; Shinde and Maddika, 2016; Song et al., 2016; Lin et al., 2017; Modica et al., 2017). A recent work involving multilayered proteomics to understand EGFR degradation revealed regulation of RAB7 trafficking by multiple PTMs (Francavilla et al., 2016) and the interacting partners of RAB7 were shown to vary with its modification by ubiquitylation and phosphorylation. In the present

work, we show yet another mode of regulation of RAB7 activity and stability through SUMO modification. A mutation at K175 of RAB7 almost completely abolished its SUMOylation, revealing this lysine to be the primary site of SUMO modification. RAB7 recruitment takes place in late phagolysosomes; however, its nucleotide exchange function is blocked by direct binding of the *S*. Typhimurium effector SopD2 to RAB7. This binding consequently limits RAB7 interaction with FYCO and RILP, thereby preventing delivery of endocytic cargo to lysosomes (D'Costa et al., 2015). The current work furthers this concept and reveals SUMOylation to be another means by which *S*. Typhimurium can potentially modulate RAB7 function. *S*. Typhimurium inhibits multiple members of the SUMOylation pathway such as UBC9 and PIAS1, and causes an overall decrease in the host SUMOylation status (Verma et al., 2015). *S*. Typhimurium may elicit global SUMO pathway alteration to block SUMOylation of proteins such as RAB7, as is evident from our data (immunoprecipitation of SUMO and RAB7, Fig. 3A). The importance of this inhibition was reflected when cells expressing a SUMOylation-deficient mutant of RAB7 (RAB7^{K175R}) were used in the study. Firstly, this mutant protein displayed a better stability compared to wild-type RAB7, which in turn appeared to undergo degradation in a proteasome-dependent way at rates faster than the SUMO-deficient mutant. RAB7 itself governs proper turnover of many cellular proteins by governing the lysosomal and proteasome degradation pathway (Sun et al., 2005; Sakane et al., 2007). However, the mechanism of RAB7 turnover is not well studied and is an area that was investigated in the current work. MG132, a drug that blocks the proteasome pathway and some members of the lysosomal pathway, was able to rescue the SUMOylation-mediated degradation of RAB7. Thus, one mode of RAB7 turnover may be through the lysosomal and proteasome machineries. Interestingly, RAB7^{K175R} was resistant to this rescue, indicating that the presence of K175 may be required for the functioning of this mechanism. RAB7 is known to also undergo ubiquitylation at K38 (Song et al., 2016). However, at present, the precise connection between SUMOylation and ubiquitylation of RAB7 remains unknown and would be an interesting avenue for future investigations. A second interesting aspect of RAB7^{K175R} was that this mutant was functionally inactive, as revealed by cell fractionation and a series of other assays. Active GTP-bound RAB7 is usually a membrane resident; in our cell fractionation experiments we observed that the localization of the mutant was not altered but it was functionally inactive. Furthermore, in line with this model, infected cells that express RAB7^{K175R} displayed a significant increase in SIF formation. These cells also showed a significantly greater co-localization of *S*. Typhimurium and RAB7^{K175R}. It was surprising, however, that the majority of RAB7^{K175R} was found in the cytoplasmic fraction. This meant that in the absence of SUMOylation, the RAB7 remained in the vicinity of *S*. Typhimurium but in a non-functional state. *S*. Typhimurium undergoes multiplication and initiates elongation of SCV into SIFs at later stages of its intracellular life. SIF formation and the maintenance of SCV largely depend on a key Salmonella pathogenecity island-2 (SPI-2) effector called SifA. A recent study has revealed that the involvement of a lysosomal adapter protein PLEKHM1 was required in the very late stages of endolysosomal maturation, governing both lysosomal degradation processes and autophagosome clearance. Interestingly, they showed that PLEKHM1 was required for SCV morphology such that *S*. Typhimurium utilized PLEKHM1 at late stages of the endolysosome. The process required the interaction of PLEKHM1 with RAB7 and *S*. Typhimurium effector SifA. In this way, *S*. Typhimurium recruited a multiprotein complex involving

PLEKHM1, RAB7 and the HOPS tethering complex, a process required for mobilization of phagolysosomal membranes to the SCV (McEwan et al., 2015). This process was also shown to be crucial for addition of the new membrane that is required by a growing SCV. In line with these studies, we observed a stronger interaction between PLEKHM1 and RAB7^{K175R} in comparison to that between PLEKHM1 and wild-type RAB7. The cellular bacterial burden as revealed by CFU assay was also higher in cells expressing RAB7^{K175R} than in cells expressing wild-type RAB7.

The importance of RAB7 SUMOylation in its involvement in other cellular processes such as regular endocytic trafficking and autophagy may require further investigation. The current work gives strong evidence that RAB7 is SUMOylated, and that this PTM contributes to the intracellular life of *S*. Typhimurium. Here, we reveal a novel mode of regulation of RAB7, dependent on SUMOylation, which is blocked by *S*. Typhimurium during its intracellular life (Fig. S7). Our results, which are summarized in the model in Fig. S7, show that SUMO-deficient RAB7 displays a stronger interaction with its cognate effector, PLEKHM1, and a weaker interaction with RILP than wild-type RAB7. These key changes to molecular mechanisms lead to better SIF formation and a more stable SCV. Together, these events allow better *S*. Typhimurium multiplication. The process may fully or partly depend on the capacity of *S*. Typhimurium to downregulate the global host SUMOylome. There may be RAB7-specific mechanisms that are also crucial to *S*. Typhimurium multiplication, but that will need further investigation. Thus, the current work gives strong evidence of a novel PTM-mediated effect on a master regulator protein, RAB7, which in turn effects the intracellular life of *S*. Typhimurium. A SUMOylation-mediated switch from non-functional to a functional state of RAB7 is a novel phenomenon and may be a crucial mode of operation of the vesicular transport system pertaining to all intracellular pathogens.

MATERIALS AND METHODS
All chemicals, unless otherwise specified, were obtained from Sigma-Aldrich. Antibodies directed against RAB7 (1:5000, R4779), EEA1 (1:2000, E4156), LAMP1 (WB 1:2000, IF 1:1000, L1418), Ubc-9 (1:5000, U2634), RNF4 (1:5000, SAB1100321), PLEKHM1 (1:200, HPA039473) and SUMO1 (1:5000, S8070) were obtained from Sigma-Aldrich. Anti-GAPDH (1:5000, 39-8600), anti-SUMO2/3 (1:1000, 51-9100), HRP-conjugated anti-rabbit (1:5000, 65-6120) and HRP-conjugated anti-mouse (1:5000, 62-6520) antibodies were obtained from Invitrogen. Anti-GFP (1:3000, ab6556), anti-RILP (1:4000, ab128616) and anti-HA (1:200, ab18181) were obtained from Abcam. Anti-SUM2/3 used for IP was obtained from Santa Cruz Biotechnology (1 µg:200 µg of lysate, sc393144), anti-active RAB7 used for IP from NewEast Bioscience (1 µg:200 µg of lysate, 26923) and anti-ubiquitin from Cell Signaling Technology (1:2000, 3993). Cy5-conjugated goat anti-rabbit IgG (1:1000, 111-175-144) was obtained from The Jackson Laboratory.

Cell culture
HCT-8 intestinal epithelial cells (ATCC, Manassas, VA, USA) (passages 2 to 25) were cultured in RPMI medium supplemented with 14 mM NaHCO$_3$, 15 mM HEPES buffer (pH 7.4), 2 mM glutamine, 1 mM sodium pyruvate, 40 mg/l penicillin, 90 mg/l streptomycin, and 10% fetal bovine serum. HeLa cells were cultured in Dulbecco's modified Eagle's medium (DMEM) containing 14 mM NaHCO$_3$, 15 mM HEPES buffer (pH 7.5), 40 mg/l penicillin, 90 mg/l streptomycin, and 10% fetal bovine serum. Cells were treated with different pharmacological drugs: MG132 at 20 mM 2 h before completion of infection, cycloheximide at 20 µM 1 h before infection until the completion of the infection process. To calculate the half-life of proteins, the level of each protein at time 0 was set as 100% and the percentage of protein remaining at each time point was calculated and plotted. Linear regression analysis of each data set was carried out using Stata software (StataCorp) and used to calculate protein half-lives (0, 4 and 8 h for control,

S. Typhimurium-infected, SUMO upregulation control and SUMO upregulation *S.* Typhimurium-infected experimental groups) and plotted using GraphPad Prism software.

Bacterial strains, plasmids and infection

Salmonella Typhimurium strain SL1344 (obtained from Beth McCormick, University of Massachusetts Medical School, MA) was grown in Luria broth (LB) at 37°C aerobically for 8 h followed by growth under stationary and hypoxic conditions overnight. These were then used to infect epithelial cells at a multiplicity of infection (MOI) of 1:40. *S.* Typhimurium expressing mCherry was constructed by transforming *S. Typhimurium* with pFPV-mCherry procured from Addgene (Addgene plasmid 20956).

Plasmids expressing RAB7–GFP, RAB7^{Q67L}, RAB7^{T22N}, GST–RAB7 were kind gifts from Dr Amit Tuli, IMTECH, Chandigarh, India, and Dr Mahak Sharma, IISER, Mohali, India. hPLEKHM1-dsRedM (Van Wesenbeeck et al., 2007; Addgene plasmid id: 73592), pcDNA3/UBC9 (Edward Yeh; Addgene plasmid id 20082), pcDNA3 HA-SUMO2 (Addgene plasmid id: 48967), pEYFP SUMO1 (Addgene plasmid id: 13380), pGEX-4T-3-mR7BD (Addgene plasmid id: 79149) were procured from Addgene (Ayaydin and Dasso, 2004; Békés et al., 2011).

Cell transfection

HCT-8 and HeLa cells were used for transfection as described previously (Srikanth et al., 2010). One day before transfection, 2.5×10^5 cells were plated in 24-well plates to obtain 80% confluence and transfected using Lipofectamine 2000 (Invitrogen, USA). Briefly, 1 µg of plasmid was diluted in Opti-MEM (Invitrogen, USA). Separately, Lipofectamine 2000 (Invitrogen, USA) was also diluted and incubated at room temperature for 5 min. Following incubation, the two mixtures were combined and incubated at room temperature for 20 min. This cocktail was added to cells with Opti-MEM and incubated without selection for 24 h.

Western blot

Cells were lysed in Laemmli buffer (20 mM Tris-HCl pH 8.0, 150 mM KCl, 10% glycerol, 5 mM MgCl$_2$ and 0.1% NP40) supplemented with Halt Protease Inhibitor Cocktail (Thermo Fisher Scientific). Protein lysates were separated using sodium dodecyl sulfate–polyacrylamide gel electrophoresis and transferred to nitrocellulose membrane. Blots were probed with antibodies against SUMO2/3, RAB7, GAPDH, LAMP1, EEA1, GFP, RNF4, SUMO1, UBC9, ubiquitin, RILP and PLEKHM1.

Immunoprecipitation

HCT-8 cells were lysed in immunoprecipitation lysis buffer (Thermo Fisher Scientific) supplemented with 20 mM NEM, 1 mM PMSF and protease inhibitor, and debris was removed by centrifugation at 15700 *g* for 10 min at 4°C. The lysates obtained were incubated with protein G sepharose beads (Sigma-Aldrich) for 30 min at 4°C on an end-to-end rotor, followed by centrifugation to remove the beads and the non-specifically bound proteins. The precleared lysate was then used to immunoprecipitate SUMO2/3- or GFP–RAB7-conjugated proteins by incubation with their respective antibodies overnight at 4°C on an end-to-end rotor. As controls, IgG antibodies raised in mouse and rabbit, and lysates from cells transfected with a plasmid expressing GFP only were used. The antibody-bound proteins were then captured using protein G sepharose beads and washed five times with lysis buffer followed by boiling in Laemmli buffer.

Immunofluorescence

Cells were grown on cover slips. For fixed-cell imaging post infection, cells were washed two times in 1× phosphate buffered saline (PBS) and fixed in 2.5% paraformaldehyde pH 7.4 for 15 min at room temperature (RT) followed by washing in PBS. Cells were permeabilized by incubation in PBS containing 0.1% saponin and 1% bovine serum albumin (PSB buffer) for 30 min. For immunostaining, cells were incubated with polyclonal rabbit anti-LAMP1 (1:1000, prepared in PSB buffer), anti-PLEKHM1 (1:200) or anti-HA for SUMO2 (1:200) for 1 h at RT and then washed three times and incubated with Cy5-conjugated goat anti-rabbit IgG (1:1000) for a further 1 h. Cells were washed three times and incubated in 4,6-diamidino-2-

phenylindole (DAPI) (1 µg/ml; Sigma-Aldrich) for 5 min. Coverslips were mounted using Slowfade mounting medium (Invitrogen). The cells were observed using a Leica confocal SP8 microscope with a 63× oil objective. Quantitation was carried out manually for the presence of SIFs. Co-localization was calculated using the Imaris software COLOC tool (Bitplane).

Gentamicin protection assay (GPA)

HCT-8 cells were infected with *S.* Typhimurium either with or without activation of SUMOylation for 1 h. The unbound bacteria were then washed off with 1× Hank's balanced salt solution (HBSS) followed by incubation in HBSS containing 100 µg/ml of gentamicin to kill any extracellular bacteria for 1 h. After 1 h of Gentamicin treatment, cells were incubated with 10 µg/ml of gentamicin until completion of infection in a complete media without pen/strep antibiotics. Following incubation, the cells were lysed using 0.1% Triton X-100 in PBS. Samples were serially diluted in sterile PBS and plated onto LB agar plates with Strep50. CFUs were calculated by counting the number of colonies obtained the next day. A countable range of 30 to 300 was utilized.

Cloning, expression and purification of RNF4 and RNF4 SIM mutant protein and SUMO-conjugated protein isolation

Wild-type RNF4 and SIM mutant RNF4 were cloned into pGEX6P1 vector and expressed in *E. coli* Rosetta cells, followed by purification using glutathione beads in 0.5 mM IPTG. The protein was further allowed to remain bound to glutathione beads. HCT-8 cells were infected with *S.* Typhimurium for 4 h. After infection, cells were washed using cold 1× PBS then incubated with lysis buffer for 15 min [10 mM HEPES pH 7.9, 1.5 mM MgCl$_2$, 10 mM KCl, 0.07% NP40, protease inhibitor (Thermo Fisher Scientific), 200 mM iodoacetamide, 20 mM NEM]. The cells were centrifuged at 13,000 rpm for 10 min at 4°C to remove the debris. The supernatant was used to isolate the SUMO2-conjugated proteins. A total of 7 mg of cell lysates were incubated with 100 µl of GST–RNF4 fusion protein overnight on a rotor at 4°C. The beads were washed five times with 50 mM Tris (pH 7.5), 250 mM NaCl, 1% NP40, 0.5% sodium deoxycholate (wash buffer) and further incubated with wash buffer containing SIM peptides (1 µg/µl) for 2 h at 4°C in an end-to-end rotor. Eluted proteins were further concentrated using the Millipore Amicon Centrifugal Filter Concentrator (Millipore). The proteins were then separated using SDS-PAGE and subjected to in-gel digestion for mass spectrometry analysis.

Liquid chromatography and mass spectrometry

The immunoprecipitated proteins were separated on 12% SDS-PAGE and gel bands were digested with trypsin (Promega Trypsin Gold) at a dilution of 1:50. In brief, gel bands were destained using 50 mM ammonium bicarbonate and 50% acetonitrile (destain buffer). Gel bands were washed six times in destain buffer to remove all the gel stain. Once bands were destained, the protein was reduced with 5 mM DTT for 30 min at 50°C. Reduced proteins were alkylated using 10 mM iodoacetamide (IAA) for 30 min at 50°C in the dark. Gel pieces were washed again with ammonium bicarbonate to remove any unused IAA. The gel pieces were dried under vacuum and MS-grade trypsin was added to the dried gel pieces at 4°C. Samples were kept on ice for 30 min to absorb trypsin and then gel pieces were incubated at 37°C for overnight digestion. After digestion, peptides were extracted in 0.1% TFA and desalted using ZipTip C18 sample prep pipette tips (Millipore) before injection into the instrument. Desalted peptides were dissolved in 98% water, 2% acetonitrile and 0.1% formic acid. Peptides were separated on a nano C18 column (Merck) with a flow rate of 300 nl/min and an increasing gradient of acetonitrile on a 45 min gradient. Tandem MS analysis was performed using a 5600 TripleTOF analyser (Ab Sciex) in information-dependent acquisition (IDA) mode. Peptides were ionized with an ionization voltage of 2100 V and nebulizer gas was used at the flow rate of 10 l/min to assist the ionization of the analytes. Multiple charged precursor ions were selected across the mass range of 300–1250 m/z and the 20 most intense peptides were fragmented in CID according to the criteria set in the IDA method with rolling collision energy. Protein identification was performed with the Mascot search engine (Matrix

Science) incorporated into ProteinPilot 4.0 (Ab Sciex). User-defined search parameters were as used to search the data set; for example, trypsin was used as protease, and two missed cleavages were allowed for the search algorithm, mass tolerance for MS and MS/MS were 50 ppm and 300 ppm, respectively. For identification of SUMOylation sites on selected protein sequence we generated an *in silico* modified SUMOylation site using ChopNSpice servers (https://chopnspice.gwdg.de/; Hsiao et al., 2009) and the resultant FASTA file were used as a database for the Paragon algorithm in a ProteinPilot search. The FASTA file was generated with the following parameters: species, *Homo sapiens*; spice sequences, SUMO2; spice site, KX; spice mode was once per fragment; include unmodified fragment as output; enzyme, trypsin (Lys/Arg but do not cleave at Pro); allow up to three protein miscleavages; allow up to one miscleavage in spice fragment; output format as FASTA (single protein sequence); mark all cleaved sites as J; retain comments in FASTA format without line breaks in FASTA output. For SUMOylated site identification by using the quantitative proteomics software MAXQUANT, all MS/MS spectra were searched against a new FASTA file that was created by ChopNSpice with the following parameters: mass tolerance of 10 ppm in MS mode and 0.8 Da in MS/MS mode; allow zero missed cleavages; consider methionine oxidation and cysteine carboxyamidomethylation as variable modifications. All high abundance peaks had to be assigned to y- or b-ion series.

Purification and *in vitro* SUMOylation of RAB7

RAB7 was expressed in *E. coli* BL21. For expression, cells were induced using 0.4 mM IPTG at 18°C overnight, supplemented with 100 µg/ml of ampicillin and purified using glutathione sepharose beads (GE Healthcare). SUMO conjugation reactions were performed with 500 nM of RAB7 protein at 37°C overnight in the presence of ATP. Other components for SUMOylation using a SUMOylation kit (Enzo Life Sciences, BML-UW8955) were added as per the manufacturer's instructions, in a 20 µl reaction volume. The reaction was stopped by adding 2× Laemmli buffer. Approximately 10 µl of sample was loaded onto SDS-PAGE, and bands stained for SUMO2. 20 µl of sample was digested in-gel for MS/MS analysis as described previously. For identification of SUMOylation sites, the method followed is described above in detail under Liquid chromatography and mass spectrometry.

Protein docking

Protein docking experiments were carried out using the ClusPro program (Comeau et al., 2004). It utilizes PIPER (Kozakov et al., 2006), a FFT-based algorithm, to perform rigid body docking by sampling billions of protein conformations and cluster the structures with lowest energy based on root-mean-square deviation (RMSD). The crystal structure of RAB7 (PDB ID: 3LAW) and SUMO2 (PDB ID: 5GHC) were selected as receptor and ligand molecules. The final models were selected for refinement and energy minimization. Models were analysed visually and those that did not display expected interactions were excluded. The analysis of results and figures were generated using UCSF Chimera (Pettersen et al., 2004).

Flow cytometry analysis

HCT-8 cells were seeded at 4×10^5 cells in a 6-well plate. 24 h after splitting, cells were transfected with GFP-tagged WT RAB7 and RAB7[K175R], along with DsRed–PLEKHM1. 24 h post transfection, cells were infected with *S.* Typhimurium for 4 h. After infection, cells were removed by incubating with trypsin for 5 min at 37°C. Cells were further spun down at 100 **g** for 5 min. Cells were resuspended in 1× PBS and kept for sorting using a FACS cell sorter (BD) based on expression of GFP for RAB7, and then on expression of DsRed for PLEKHM1.

Cell fractionation

A cell fractionation assay was performed following the protocol of Seaman et al. (2009). HCT-8 cells were grown in 10 cm dishes. Cells were transfected with constructs expressing WT RAB7 and RAB7[K175R]. Following transfection, cells were infected with *S.* Typhimurium for 7 h, with one plate was kept as uninfected control. Post-infection, cells were washed with 1× PBS. They were snap-frozen using liquid nitrogen and then immediately thawed on the bench. Cells were scraped using 0.5 ml buffer

(0.1 M MES-NaOH pH 6.5, 1 mM magnesium acetate, 0.5 mM EGTA, 200 µM sodium orthovanadate, 0.2 M sucrose). The lysates were centrifuged for 10 min at 10,000 **g**. Cytosol-containing supernatants were kept separately. The pellets, containing the membranous fraction, were solubilized in 0.5 ml of fractionation lysis buffer (50 mM Tris-HCl pH 7.4, 150 mM NaCl, 1 mm EDTA, 1% Triton X-100, 0.1% SDS) and re-centrifuged for 10 min at 10,000 **g**. Equal amount of both cytosolic and membrane fractions were subjected to SDS-PAGE and western blot.

RAB7 activation assay

A RAB7 activation assay was carried out using an immunoprecipitation-aided methodology based on a protocol from NewEast Biosciences (catalogue #82501). Briefly, 2 mg of protein lysates were incubated overnight at 4°C with 1 µl of antibody specific to active RAB7, in an end-to-end rotor. The following day, the lysates were incubated with protein G sepharose beads for 4 h at 4°C in an end-to-end rotor. The beads were pelleted down at 5000 **g** for 1 min. The supernatant was removed and the beads were washed three times with lysis buffer (30 ml of 250 mM Tris-HCl pH 8, 750 mM NaCl, 50 mM MgCl2, 5 mM EDTA, 5% Triton X-100.) followed by centrifugation and aspiration. After the last wash, beads were resuspended with 1× Laemmli buffer, samples loaded onto an SDS-PAGE gel and the resulting bands labelled with anti-RAB7 (polyclonal) antibody by immunoblotting.

GST–RILP pulldown assay

The protocol for purification of GST–RILP protein was described previously (Romero Rosales et al., 2009). For protein expression and purification, bacterial expression vectors encoding GST or GST-tagged RILP were transformed into *E. coli* BL21. Primary culture of a transformed colony was set up for 12 h at 37°C in LB broth containing the plasmid vector and selection antibiotic. Secondary culture was set up from primary culture and incubated at 37°C in LB broth until the OD_{600} reached 0.6, then the protein was induced with 0.5 mM IPTG for 4 h at 30°C. After induction, the bacterial culture was pelleted down and washed with ice cold 1× PBS. The pellet was resuspended in 5 ml of buffer A (25 mM Tris-HCl pH 7.4, 1 M NaCl, 0.5 mM EDTA, 1 mM DTT, 0.1% Triton X-100, complete protease inhibitor). The culture was sonicated and spun down at 12633 **g** for 10 min at 4°C. The supernatant was transferred to a 15 ml conical tube and 5 ml of buffer A was added. Cells were lysed with pulldown lysis buffer (20 mM HEPES pH 7.4, 100 mM NaCl, 5 mM MgCl2, 1% Triton X-100, complete protease inhibitor), lysates were incubated for 1 h at RT with 250 µl of glutathione–sepharose beads, followed by spin-down at 500 **g** to pellet the beads. The beads were washed twice with ice-cold buffer A. Next, lysates prepared from HCT-8 cells infected with *S.* Typhimurium and transfected with WT RAB7 and RAB7[K175R] were passed through 30 µg of GST or GST–RILP matrix overnight in an end-to-end rotor. Samples were washed three times with pulldown lysis buffer, elution was performed by boiling the samples in 40 µl of 1× Lamelli buffer, and 20 µl was loaded onto SDS-PAGE for analysis.

Statistics

All results expressed as the mean±s.e.m. from an individual experiment done in triplicate. Data were analysed with standard two-tailed Student's *t*-test, and *P*-values <0.05–0.0001 were considered statistically significant. We evaluated the statistics using GraphPad Prism software.

Competing interests

The authors declare no competing or financial interests.

Author contributions

Conceptualization: C.V.S.; Methodology: N.K., S.V., C.V.S.; Software: G.M., S.P., V.K., N.S.; Validation: G.M., P.G., P.M., C.V.S.; Formal analysis: C.V.S.; Investigation: G.M., S.P., N.K., S.V.; Resources: C.V.S.; Data curation: M.S., C.V.S.;

References
Ayaydin, F. and Dasso, M. (2004). Distinct in vivo dynamics of vertebrate SUMO paralogues. *Mol. Biol. Cell* **15**, 5208-5218.
Bakowski, M. A., Braun, V. and Brumell, J. H. (2008). Salmonella-containing vacuoles: directing traffic and nesting to grow. *Traffic* **9**, 2022-2031.
Baldeón, M. E., Ceresa, B. P. and Casanova, J. E. (2001). Expression of constitutively active Rab5 uncouples maturation of the Salmonella-containing vacuole from intracellular replication. *Cell. Microbiol.* **3**, 473-486.
Békés, M., Prudden, J., Srikumar, T., Raught, B., Boddy, M. N. and Salvesen, G. S. (2011). The Dynamics and mechanism of SUMO chain deconjugation by SUMO-specific proteases. *J. Biol. Chem.* **286**, 10238-10247.
Beuzón, C. R., Méresse, S., Unsworth, K. E., Ruíz-Albert, J., Garvis, S., Waterman, S. R., Ryder, T. A., Boucrot, E. and Holden, D. W. (2000). Salmonella maintains the integrity of its intracellular vacuole through the action of SifA. *EMBO J.* **19**, 3235-3249.
Bhan, M. K., Bahl, R. and Bhatnagar, S. (2005). Typhoid and paratyphoid fever. *Lancet* **366**, 749-762.
Bruderer, R., Tatham, M. H., Plechanovova, A., Matic, I., Garg, A. K. and Hay, R. T. (2011). Purification and identification of endogenous polySUMO conjugates. *EMBO Rep.* **12**, 142-148.
Brumell, J. H. and Grinstein, S. (2004). Salmonella redirects phagosomal maturation. *Curr. Opin. Microbiol.* **7**, 78-84.
Comeau, S. R., Gatchell, D. G., Vajda, S. and Camacho, C. J. (2004). ClusPro: a fully automated algorithm for protein-protein docking. *Nucleic Acids Res.* **32**, W96-W99.
D'Costa, V. M., Braun, V., Landekic, M., Shi, R., Proteau, A., Mcdonald, L., Cygler, M., Grinstein, S. and Brumell, J. H. (2015). Salmonella disrupts host endocytic trafficking by SopD2-mediated inhibition of RAB7. *Cell Rep.* **12**, 1508-1518.
Domingues, P., Golebiowski, F., Tatham, M. H., Lopes, A. M., Taggart, A., Hay, R. T. and Hale, B. G. (2015). Global Reprogramming of Host SUMOylation during Influenza Virus Infection. *Cell Rep.* **13**, 1467-1480.
Drecktrah, D., Knodler, L. A., Howe, D., Steele-Mortimer, O. (2007). Salmonella trafficking is defined by continuous dynamic interactions with the endolysosomal system. *Traffic* 8, 212-225.
Flotho, A. and Melchior, F. (2013). Sumoylation: a regulatory protein modification in health and disease. *Annu. Rev. Biochem.* **82**, 357-385.
Forest, C. G., Ferraro, E., Sabbagh, S. C. and Daigle, F. (2010). Intracellular survival of Salmonella enterica serovar Typhi in human macrophages is independent of Salmonella pathogenicity island (SPI)-2. *Microbiology* **156**, 3689-3698.
Francavilla, C., Papetti, M., Rigbolt, K. T., Pedersen, A. K, Sigurdsson, J. O., Cazzamali, G., Karemore, G., Blagoev, B. and Olsen, J. V. (2016). Multilayered proteomics reveals molecular switches dictating ligand-dependent EGFR trafficking. *Nat. Struct. Mol. Biol.* **23**, 608-618.
Galán, J. E. (1996). Molecular genetic bases of Salmonella entry into host cells. *Mol. Microbiol.* **20**, 263-271.
Gareau, J. R., Reverter, D. and Lima, C. D. (2012). Determinants of Small Ubiquitin-like Modifier 1 (SUMO1) protein specificity, E3 ligase, and SUMO-RanGAP1 binding activities of nucleoporin RanBP2. *J. Biol. Chem.* **287**, 4740-4751.
Girard, E., Chmiest, D., Fournier, N., Johannes, L., Paul, J.-L., Vedie, B. and Lamaze, C. (2014). RAB7 is functionally required for selective cargo sorting at the early endosome. *Traffic* **15**, 309-326.
Groocock, L. M., Nie, M., Prudden, J., Moiani, D., Wang, T., Cheltsov, A., Rambo, R. P., Arvai, A. S. et al. (2014). RNF4 interacts with both SUMO and nucleosomes to promote the DNA damage response. *EMBO Rep.* **15**, 601-608.
Harrison, R. E., Brumell, J. H., Khandani, A., Bucci, C., Scott, C. C., Jiang, X., Finlay, B. B. and Grinstein, S. (2004). Salmonella impairs RILP recruitment to RAB7 during maturation of invasion vacuoles. *Mol. Biol. Cell* **15**, 3146-3154.
Hendriks, I. A., Treffers, L. W., Verlaan-de Vries, M., Olsen, J. V. and Vertegaal, A. C. O. (2015). SUMO-2 orchestrates chromatin modifiers in response to DNA damage. *Cell Rep.* **10**, 1778-1791.
Hsiao, H.-H., Meulmeester, E., Frank, B. T. C., Melchior, F. and Urlaub, H. (2009). "ChopNSpice," a mass spectrometric approach that allows identification of endogenous small ubiquitin-like modifier-conjugated peptides. *Mol. Cell. Proteomics* **8**, 2664-2675.
Jordens, I., Fernandez-Borja, M., Marsman, M., Dusseljee, S., Janssen, L., Calafat, J., Janssen, H., Wubbolts, R. and Neefjes, J. (2001). The RAB7 effector protein RILP controls lysosomal transport by inducing the recruitment of dynein-dynactin motors. *Curr. Biol.* **11**, 1680-1685.
Kozakov, D., Brenke, R., Comeau, S. R. and Vajda, S. (2006). PIPER: an FFT-based protein docking program with pairwise potentials. *Proteins* **65**, 392-406.
Lin, X., Zhang, J., Chen, L., Chen, Y., Xu, X., Hong, W. and Wang, T. (2017). Tyrosine phosphorylation of RAB7 by Src kinase. *Cell. Signal.* **35**, 84-94.
Madan, R., Krishnamurthy, G. and Mukhopadhyay A. (2008). SopE-Mediated Recruitment of Host Rab5 on Phagosomes Inhibits Salmonella Transport to Lysosomes. In *Autophagosome and Phagosome* (ed. V. Deretic), pp. 417-437. Totowa, NJ: Humana Press.
Madan, R., Rastogi, R., Parashuraman, S. and Mukhopadhyay, A. (2012). Salmonella acquires Lysosome-associated Membrane Protein 1 (LAMP1) on phagosomes from Golgi via SipC protein-mediated recruitment of host Syntaxin6. *J. Biol. Chem.* **287**, 5574-5587.
McEwan, D. G., Richter, B., Claudi, B., Wigge, C., Wild, P., Farhan, H., McGourty, K., Coxon, F. P., Franz-Wachtel, M., Perdu, B. et al. (2015). PLEKHM1 regulates salmonella-containing vacuole biogenesis and infection. *Cell Host Microbe* **17**, 58-71.
McGourty, K., Thurston, T. L., Matthews, S. A., Pinaud, L., Mota, L. J. and Holden, D. W. (2012). Salmonella inhibits retrograde trafficking of mannose-6-phosphate receptors and lysosome function. *Science* **338**, 963-967.
Modica, G., Skorobogata, O., Sauvageau, E., Vissa, A., Yip, C. M., Kim, P. K., Wurtele, H. and Lefrancois, S. (2017). RAB7 palmitoylation is required for efficient endosome-to-TGN trafficking. *J. Cell Sci.* **130**, 2579-2590.
Mustfa, S. A., Singh, M., Suhail, A., Mohapatra, G., Verma, S., Chakravorty, D., Rana, S., Rampal, R., Dhar, A., Saha, S. et al. (2017). SUMOylation pathway alteration coupled with downregulation of SUMO E2 enzyme at mucosal epithelium modulates inflammation in inflammatory bowel disease. *Open Biol.* **7**, 170024.
Ohlson, M. B., Huang, Z., Alto, N. M., Blanc, M.-P., Dixon, J. E., Chai, J. and Miller, S. I. (2008). Structure and function of Salmonella SifA indicate that its interactions with SKIP, SseJ, and RhoA family GTPases induce endosomal tubulation. *Cell Host Microbe* **4**, 434-446.
Pettersen, E. F., Goddard, T. D., Huang, C. C., Couch, G. S., Greenblatt, D. M., Meng, E. C. and Ferrin, T. E. (2004). UCSF Chimera—a visualization system for exploratory research and analysis. *J. Comput. Chem.* **25**, 1605-1612.
Ribet, D., Hamon, M., Gouin, E., Nahori, M.-A., Impens, F., Neyret-Kahn, H., Gevaert, K., Vandekerckhove, J., Dejean, A. and Cossart, P. (2010). Listeria monocytogenes impairs SUMOylation for efficient infection. *Nature* **464**, 1192-1195.
Rink, J., Ghigo, E., Kalaidzidis, Y. and Zerial, M. (2005). Rab conversion as a mechanism of progression from early to late endosomes. *Cell* **122**, 735-749.
Romero Rosales, K., Peralta, E. R., Guenther, G. G., Wong, S. Y., Edinger, A. L. and Margolis, B. (2009). RAB7 activation by growth factor withdrawal contributes to the induction of apoptosis. *Mol. Biol. Cell* **20**, 2831-2840.
Sakane, A., Hatakeyama, S. and Sasaki, T. (2007). Involvement of Rabring7 in EGF receptor degradation as an E3 ligase. *Biochem. Biophys. Res. Commun.* **357**, 1058-1064.
Sakin, V., Richter, S. M., Hsiao, H. H., Urlaub, H. and Melchior, F. (2015). Sumoylation of the GTPase Ran by the RanBP2 SUMO E3 Ligase Complex. *J. Biol. Chem.* **290**, 23589-23602.
Sampson, D. A., Wang, M. and Matunis, M. J. (2001). The Small Ubiquitin-like Modifier-1 (SUMO-1) consensus sequence mediates Ubc9 binding and is essential for SUMO-1 modification. *J. Biol. Chem.* **276**, 21664-21669.
Seaman, M. N. J., Harbour, M. E., Tattersall, D., Read, E. and Bright, N. (2009). Membrane recruitment of the cargo-selective retromer subcomplex is catalysed by the small GTPase RAB7 and inhibited by the Rab-GAP TBC1D5. *J. Cell Sci.* **122**, 2371-2382.
Shinde, S. R. and Maddika, S. (2016). PTEN modulates EGFR late endocytic trafficking and degradation by dephosphorylating RAB7. *Nat. Commun.* **7**, 10689.
Sloan, E., Tatham, M. H., Groslambert, M., Glass, M., Orr, A., Hay, R. T. and Everett, R. D. (2015). Analysis of the SUMO2 Proteome during HSV-1 Infection. *PLoS Pathog.* **11**, e1005059.
Soldati, T., Rancaño, C., Geissler, H. and Pfeffer, S. R. (1995). RAB7 and Rab9 are recruited onto late endosomes by biochemically distinguishable processes. *J. Biol. Chem.* **270**, 25541-25548.
Song, P., Trajkovic, K., Tsunemi, T. and Krainc, D. (2016). Parkin modulates endosomal organization and function of the endo-lysosomal pathway. *J. Neurosci.* **36**, 2425-2437.
Srikanth, C. V., Wall, D. M., Maldonado-Contreras, A., Shi, H. N., Zhou, D., Demma, Z., Mumy, K. L. and Mccormick, B. A. (2010). Salmonella pathogenesis and processing of secreted effectors by caspase-3. *Science* **330**, 390-393.
Srikanth, C. V., Mercado-Lubo, R., Hallstrom, K. and Mccormick, B. A. (2011). Salmonella effector proteins and host-cell responses. *Cell. Mol. Life Sci.* **68**, 3687-3697.

Steele-Mortimer, O., Méresse, S., Gorvel, J.-P., Toh, B.-H. and Finlay, B. B. (1999). Biogenesis of Salmonella typhimurium-containing vacuoles in epithelial cells involves interactions with the early endocytic pathway. *Cell. Microbiol.* **1**, 33-49.

Sun, Y., Büki, K. G., Ettala, O., Vääräniemi, J. P. and Väänänen, H. K. (2005). Possible role of direct Rac1-RAB7 interaction in ruffled border formation of osteoclasts. *J. Biol. Chem.* **280**, 32356-32361.

Van Wesenbeeck, L., Odgren, P. R., Coxon, F. P., Frattini, A., Moens, P., Perdu, B., Mackay, C. A., Van Hul, E., Timmermans, J.-P., Vanhoenacker, F. et al. (2007). Involvement of PLEKHM1 in osteoclastic vesicular transport and osteopetrosis in incisors absent rats and humans. *J. Clin. Investig.* **117**, 919-930.

Vanlandingham, P. A. and Ceresa, B. P. (2009). RAB7 regulates late endocytic trafficking downstream of multivesicular body biogenesis and cargo sequestration. *J. Biol. Chem.* **284**, 12110-12124.

Verma, S., Mohapatra, G., Ahmad, S. M., Rana, S., Jain, S., Khalsa, J. K. and Srikanth, C. V. (2015). Salmonella engages host microRNAs to modulate SUMOylation: a new arsenal for intracellular survival. *Mol. Cell. Biol.* **35**, 2932-2946.

Vertegaal, A. C. O., Andersen, J. S., Ogg, S. C., Hay, R. T., Mann, M. and Lamond, A. I. (2006). Distinct and overlapping sets of SUMO-1 and SUMO-2 target proteins revealed by quantitative proteomics. *Mol. Cell. Proteomics* **5**, 2298-2310.

Wachtel, R., Bräuning, B., Mader, S. L., Ecker, F., Kaila, V. R. I., Groll, M. and Itzen, A. (2018). The protease GtgE from Salmonella exclusively targets inactive Rab GTPases. *Nat. Commun.* **9**, 44.

Wu, Y.-W., Goody, R. S., Abagyan, R. and Alexandrov, K. (2009). Structure of the disordered C terminus of RAB7 GTPase induced by binding to the Rab geranylgeranyl transferase catalytic complex reveals the mechanism of Rab prenylation. *J. Biol. Chem.* **284**, 13185-13192.

Zilio, N., Williamson, C. T., Eustermann, S., Shah, R., West, S. C., Neuhaus, D. and Ulrich, H. D. (2013). DNA-dependent SUMO modification of PARP-1. *DNA Repair* **12**, 761-773.